Corrosion Science 217 (2023) 111114

Contents lists available at ScienceDirect

Corrosion Science

journal homepage: www.elsevier.com/locate/corsci

In situ, real-time imaging of redox-active species on Al/Cu galvanic couple and corrosion inhibition with 2-mercaptobenzimidazole and octylphosphonic acid

Dževad K. Kozlica [a,b,1], Brenda Hernández-Concepción [c,2], Javier Izquierdo [c,d,*,3], Ricardo M. Souto [c,d,4], Ingrid Milošev [a,**,5]

[a] Jožef Stefan Institute, Department of Physical and Organic Chemistry, SI-1000 Ljubljana, Slovenia
[b] Jožef Stefan International Postgraduate School, SI-1000 Ljubljana, Slovenia
[c] Department of Chemistry, Universidad de La Laguna, 38200 La Laguna, Tenerife, Spain
[d] Institute of Material Science and Nanotechnology, Universidad de La Laguna, 38200 La Laguna, Tenerife, Spain

ARTICLE INFO

Keywords:
Aluminum Copper
Scanning electrochemical microscopy (SECM)
Scanning vibrating electrode technique (SVET)
Oxygen reduction Neutral inhibition

ABSTRACT

In situ localized electrochemical activity in the Al/Cu galvanic pair at the corrosion potential in an aggressive chloride electrolyte was investigated, along with the effect of the organic inhibitors 2-mercaptobenzimidazole (MBI) and octylphosphonic acid (OPA) on arresting the corresponding corrosion processes. Scanning electrochemical microscopy (SECM) and the scanning vibrating electrode technique (SVET) were used to discern local anodic and cathodic sites at the surface. The electrochemical activity in the galvanic pair was greatly reduced when the copper surface was covered with an MBI-containing film. SECM was successfully applied to visualize spatially resolved differences in local electrochemical activity related to the inhibitor action.

1. Introduction

To find an effective and reliable corrosion inhibitor for aluminum alloy (AA) 2024, which is widely used as a structural material in automotive, aerospace and construction industries due to its very high strength-to-weight ratio, it is crucial to understand the mechanism that governs the corrosion processes and corrosion inhibition. This aluminum alloy shows a predominance of copper-rich intermetallic particles (IMPs), Al_2Cu and Al_2CuMg [1,2], with an average size of 7.6 ± 5.2 μm [3]. Interestingly, a similar size is found for the T1 phases (Al_2CuLi) common in third-generation aluminum-based alloys which have higher lithium content, yielding excellent mechanical properties although they are susceptible to severe localized corrosion [4–6]. The crucial aspects of pit initiation, propagation or repassivation mechanisms are still unveiled, but it is widely accepted that the key role is played by the microgalvanic coupling existing between IMPs and the surrounding matrix. Therefore, addressing and controlling the localized electrochemical corrosion response (i.e., accurately measuring the potentials and currents) at these sites is particularly challenging. Since the degradation of AA2024 is mainly due to the local galvanic coupling between the IMPs and the surrounding matrix, a reasonable approach would be to mimic the intermetallic phases of the AA2024 system by testing a suitable galvanic couple model such as Al/Cu to provide key information to understand better the behavior of associated alloy systems.

Heterocyclic organic compounds containing nitrogen, sulfur, phosphorus and oxygen atoms are widely recognized as protecting metals from dissolution due to the ability of these heteroatoms to readily form bonds with metals such as aluminum [7–9] and copper [10–13]. The use of organic inhibitors is of immense technical value in corrosion

* Corresponding author at: Department of Chemistry, Universidad de La Laguna, 38200 La Laguna, Tenerife, Spain.
** Corresponding author.
E-mail addresses: jizquier@ull.edu.es (J. Izquierdo), ingrid.milosev@ijs.si (I. Milošev).
[1] https://orcid.org/0000-0003-1246-5692
[2] https://orcid.org/0000-0002-2305-9545
[3] https://orcid.org/0000-0003-3287-9403
[4] https://orcid.org/0000-0001-9429-5513
[5] https://orcid.org/0000-0002-7633-9954

https://doi.org/10.1016/j.corsci.2023.111114
Received 20 January 2023; Received in revised form 10 March 2023; Accepted 15 March 2023
Available online 17 March 2023

protection, which is reflected not only in inhibiting the dissolution of metal substrates, but also in providing anchoring points for the chemical bond between the metal oxyhydroxide and polymer coatings. We have previously shown [14], using classical electrochemical techniques and surface characterization methods, that 2-mercaptobenzimidazole (MBI) is a good inhibitor for Cu but not for Al, whereas octylphosphonic acid (OPA) behaves in an opposite way. In addition, although OPA itself did not efficiently inhibit Cu corrosion, it synergistically boosted copper inhibition when added to MBI [15]. It was revealed that the presence of chloride ions significantly promotes the synergistic effect because they play a dual role in the formation of a thick inhibitory film on copper, i.e., chloride ions simultaneously act as promoters and reactants, excluding their pure catalytic role [16].

Most of the knowledge on electrochemical corrosion and the prediction of materials performance is still gathered from conventional electrochemical techniques. However, these methods provide limited information on the electrochemical behavior at corrosion initiation sites or defects and lack sufficient spatial resolution (i.e., they provide information on the corrosion rates averaged over the entire surface), which is a key element of a rigorous mechanistic understanding. Scanning microelectrochemical techniques, such as the scanning vibrating electrode technique (SVET) and scanning electrochemical microscopy (SECM), fill this gap by providing in situ electrochemical information about the reactivity of corrosion processes simultaneously resolved in space and time. Although SVET is very powerful at distinguishing between anodic and cathodic sites in a corrosion system, it is virtually incapable of chemically discerning the species involved. On the other hand, SECM is a very attractive technique capable of obtaining high electrochemical resolution and specificity since the measuring probe can be configured to specifically monitor a certain chemical species. Therefore, it has found application for microscopic chemical imaging, where the pixels of the final image are obtained by successive local measurements throughout a raster scan. The oxygen reduction reaction (ORR) and hydrogen evolution reaction (HER) can be monitored by redox conversion using amperometric SECM, since their corresponding conversion potentials at a platinum tip lie within the stability range of water [17–19]. Additionally, the probes can image and distinguish between insulating and conducting areas, as well as reactive and passive sites, which can be exploited to study the corrosion resistance of samples treated with an inhibitor and their hampered reactivity due to the presence of an inhibitor film.

Several corrosion and inhibitor studies have already been carried out on Al/Cu galvanic coupling systems involving the use of microelectrochemical techniques, in particular SVET and SECM [20–28]. Snihirova et al. [20] observed the synergistic effect of several organic mixtures on an Al/Cu/Mg model, among which the greatest synergy was found for the mixture of 2,5-dimercapto-1,3,4-thiadiazolate (DMDT) + 8-hydroxyquinoline (8-HQ). Another inhibitory effect was revealed by Coelho et al. [24] on the Al/Cu model for the combination of 1,2,3-benzotriazole (BTA) and $CeCl_3$. The authors suggested that a protective phase of $Ce(OH)_3$ precipitated on a previously formed Cu-BTA film. The local distribution of current densities and pH values before and after the corrosion inhibition by cerium cinnamate was measured in coupled Al_2Cu/Al and Al_3Fe/Al models [21]. While adsorbed cerium cinnamate mainly influenced the corrosion inhibition on Al_3Fe/Al, the precipitation of cerium oxide/hydroxide inhibited activity on Al_2Cu/Al surface. Izquierdo et al. [27] investigated the cathodic inhibition of the Fe/Cu galvanic couple with the BTA inhibitor by dual potentiometric/amperometric operation in SECM and SVET. The results revealed that the BTA-containing layer formed on the Cu surface shifted the cathodic sites to the less noble iron surface, originally the anodic site, rendering Cu electrochemically inactive. While this effect is quite expected for inhibited galvanic surfaces and has a basis in electrochemical theory, the same effect is not reported to occur on bare galvanic coupling substrates. The literature also reports research on other galvanic systems, including Au/Cu [25], Fe/Mg [29], Cu/Ti [30], Zn/Cu [31] and Zn/Fe [22,32].

In this study, we contribute to advancing the understanding of activation and inhibition effects on surface properties through detailed in situ localized monitoring and characterization of film formation and degradation of the MBI and OPA corrosion inhibitor layers formed at the metal-liquid interface of an Al/Cu galvanic couple. For this purpose, three different operating modes of the SECM were used, namely the substrate generation-tip collection (SG-TC), redox-competition (RC) and feedback modes. Hydrogen evolution has been observed from propagating pits on aluminum, while an oxygen reduction response was recorded on copper at the free corrosion potential in the presence of an aggressive electrolyte such as 0.5 M NaCl. Additionally, SVET was used as a complementary method to the experiments performed with SECM.

Evidence of anomalous cathodic activity in the vicinity of the corroding pits has been found on the surface of anodically-activated Al (i.e., Al that is galvanically coupled to Cu), with SVET and the RC mode of SECM. Furthermore, we describe some possibilities and limitations regarding using the SECM for measurements on an Al/Cu galvanic pair, depending on whether there is active galvanic interaction under physical or only electrical contact. Additionally, the conditions under which the tip of the Pt microelectrode is blocked due to the adsorption of inhibitor molecules or the precipitation of corrosion products in the immediate vicinity of the metal-electrolyte interface are presented, and an adequate experimental setup is proposed to avoid this undesirable effect.

We believe that this work yields significant advances in basic research related to electrochemical phenomena at metal-electrolyte interfaces that will solve some important practical problems. These are mainly the unhindered monitoring of complex corrosion processes, as well as the discovery of new effective inhibitor molecules applied to galvanic systems that will contribute to the final protection of AA2024, which is an indispensable material in the automotive and aeronautical industry.

2. Methods

2.1. Materials, substrate preparation and chemicals

To investigate the interaction between corrosion inhibitors and the matrix and Cu-rich intermetallic particles in Al alloys, a simple galvanic coupling model consisting of an aluminum/copper (Al/Cu) pair was built. Fig. S1 illustrates the working electrode prepared from Al (99.0 %) and Cu (99.9 %) pure metals purchased from Goodfellow. The diameter of the Al disc was 14 mm. A 5 mm diameter hole was drilled in its center, into which the copper disc was mechanically inserted. The assembly of the two metals originated a perfectly joined interface, avoiding crevice formation and surface defects. Once prepared, this physically-connected Al/Cu sample was mounted into an insulating Epofix (Struers, Ballerup, Denmark) resin sleeve (cf. Fig. S2a in the Supplementary material). A second type of Al/Cu sample was mounted on an epoxy resin consisting of physically separated Al and Cu disks (Fig. S2b). For the galvanic coupling experiments, the two electrodes embedded in the resin could be electrically connected at the back of the mount. Before SVET and SECM measurements, these samples were ground in water with SiC paper to 4000 grit. The resulting surfaces were ultrasonically cleaned in absolute ethanol for 3 min, rinsed thoroughly with Millipore deionized water and dried under nitrogen gas flow. The electrochemical cell was constructed by gluing a cylindrical plastic body onto the epoxy resin, creating a small flat cell with an internal volume of approx. 4 mL. The sample was located at the bottom of the measuring cell, thus exposing the upper surface upwards to the test solution, as shown in Fig. S3. In this case, the samples could be studied using scanning electrochemical techniques and treated with the inhibitors in the same small cell after electrolyte exchange. The chemicals used for Cu and Al modification were sodium chloride and sodium perchlorate as aggressive and background electrolytes (reagent grade, supplied by Fisher Scientific), and 2-

mercaptobenzimidazole (MBI, 98% purity, supplied by Sigma Aldrich) and octylphosphonic acid (OPA, p 98 % purity, supplied by Ark Pharm, Inc.) as corrosion inhibitors. All reagents were used as received without further modification.

2.2. SVET instrumentation and experimental procedure

The Scanning Vibrating Electrode Technique (SVET) (Fig. S3a) was used to detect local anodic and cathodic activities above the Al/Cu galvanic pairs spontaneously corroding at the free corrosion potential. SVET detects electrochemical information in the form of small potential variations in the solution, which are associated with the ion fluxes due to oxidation and reduction reactions occurring at the active surface [23,33]. SVET experiments were performed using a system manufactured by Applicable Electronics Inc. (Forestdale, MA, USA). The vibrating probe consisted of Pt/Ir (80 %/20 %) wires insulated with Paralene C® except for the tip, which was platinized to produce a spherical deposit of platinum black with a diameter of 20 μm which served as the sensor. Two Pt wires placed in the bulk of the solution were employed as signal and reference electrodes. Since MBI is known to adsorb on Pt, resulting in partial blockage of the active surface of the probe [34], its stability and reproducibility were regularly checked by monitoring its capacitance to vary less than 10% from the value obtained after platinization.

Our focus was not on monitoring the whole surface but mainly on the Al/Cu interface and near interface regions. The analysed region is representative of the Al/Cu interface as checked by inspection under an optical microscope after completing each experiment. The mapping of the electrochemical activity was carried out in a constant height regime with an average distance of 100 μm between the microelectrode and the sample surface, which was determined using a video-microscope system. In addition to establishing the tip-sample distance, the video-camera was also used to monitor the movement of the vibrating electrode over the sample during operation and to record optical images of the substrate surface in situ. The measurements were made with the electrode tip vibrating normally and parallel (frequencies of 170 and 70 Hz, respectively) to the sample embedded horizontally in the epoxy resin and facing upwards (the electrochemical cell is shown in Fig. S3a). Microelectrochemical measurements were performed at room temperature under naturally aerated conditions in 10 mM NaCl solution containing a 1 mM concentration of the MBI or OPA inhibitors or simply in a 10 mM NaCl solution. The pH of MBI-containing NaCl was 5.5, and that of OPA-containing was adjusted to 7 [14,15].

The Al/Cu pair samples used for the SVET measurements were of the type with the physical connection between the Al and Cu metals. The in situ measurements of corrosion inhibition consisted of two steps: first, the measurement cell was filled with a solution of composition 1 mM MBI or OPA + 10 mM NaCl solution (thus conforming a reservoir of the inhibitor) for 24 h, and next the solution was replaced with 10 mM NaCl (that is, without inhibitor reservoir) for 12 h. The electrochemical activity was monitored throughout the complete immersion period. Additionally, a control sample (blank) was monitored for corrosion in 10 mM NaCl for 12 h.

2.3. SECM instrumentation and experimental procedure

SECM measurements were performed with a Sensolytics scanning electrochemical microscope (Bochüm, Germany). The system was placed inside a Faraday cage placed on a vibration isolation table to prevent electrical and acoustic noise as well as mechanical vibrations. The electrochemical interface was a bipotentiostat; however, the system was always operated in the three-electrode configuration in which the Al/Cu couple sample was left unbiased (i.e., the samples were at their corresponding OCP or mixed galvanic potential) during measurements. A commercial platinum microelectrode of 10 μm-radius was used as the working electrode. The size of the SECM tip defines the spatial resolution of the measurements. An Ag/AgCl, KCl (sat.) and platinum wire were employed as a reference and auxiliary electrodes, respectively, completing the electrochemical cell (Fig. S3b). Unless otherwise stated, all potentials values in the manuscript are referred to this reference electrode. The distance between the tip and the substrate was determined by slowly approaching the tip towards the surface of the Al/Cu sample over the resin area surrounding the metals, and simultaneously recording the approach curve (i.e., the measured current at the microelectrode vs. Z displacement of the tip) operated in negative feedback mode. For that purpose, ferrocene-methanol (FcMeOH, 0.5 mM) dissolved in the $NaClO_4$ (0.1 M) test electrolyte acted as an electrochemical mediator at the tip. To enable the oxidation of the ferrocene-methanol, the tip was held at a constant potential of + 0.50 V (Ag/AgCl), corresponding to the oxidation of the iron core of the complex from Fe(II) to Fe(III). From fitting the measured negative feedback plot to the theoretical model, for which the reduction of the mediator on the surface was assumed to be under kinetic control, the exact distance between the tip and the sample was determined. During the recording of the approach curve, the microelectrode was stopped when the measured tip current was equal to 50 % of the diffusion-limited current in the bulk of the electrolyte. Therefore, according to the fitting procedure, the microelectrode was placed 10 μm above the substrate. This value was taken as the operating distance for SECM mapping without any additional retraction of the tip from the surface. Sufficiently high surface resolution is achieved by selecting significantly smaller areas for imaging and rasterizing the tip over the sample at heights equal to one tip diameter or below. Since MBI is known to adsorb on Pt, resulting on partial blockage of the active surface of the microelectrode [35], the stability and reproducibility of the tip were regularly checked by recording a cyclic voltammogram in the 0.5 mM FcMeOH + 0.1 M $NaClO_4$ test electrolyte.

The tip potential was set at different values to monitor the local concentrations of the different species involved in the corrosion process. The effect of the negative feedback character was used to monitor the formation of insulating films on metal surfaces, revealing the effectiveness of corrosion inhibition. The experiments performed in feedback mode were carried out with the tip potential set at + 0.50 V using FcMeOH in solution as a mediator. In the case of an insulator, the proximity to the sample surface hindered the diffusion of the mediator to the measuring tip, resulting in the measurement of a smaller current at the tip than in the bulk of the electrolyte. The sample generation/tip collection (SG/TC) mode was used without adding a redox mediator to the solution. Since corroding aluminum releases H_2 molecules from the anodic sites (i.e., pits), this species can be imaged directly on the Pt tip when biased at an appropriate potential value. Therefore, the microelectrode was biased at 0.0 V to image the currents corresponding to the oxidation of H_2 to H^+ ions. On the other hand, SECM could also monitor the reduction of dissolved oxygen in the so-called redox competition mode after the tip was biased at − 0.70 V (vs. Ag/AgCl). In this mode, the sites consuming oxygen on the sample will compete for ORR with the biased microelectrode, resulting in the measurement of smaller currents at the tip. It should be emphasized that the currents measured at the tip, which come from the electroreduction of oxygen or the oxidation of ferrocene-methanol, are sensitive to the distance from the tip to the substrate and to the diffusion of the chemical species; hence the surface topography can influence the measurements as if it were a negative feedback effect.

All measurements were made by moving the tip in an XY plane parallel to the sample at a fixed height, even when the tip passed over a defective area, in which case the substrate surface was effectively at a greater distance from the tip. *In situ* images were acquired by moving the microelectrode in a raster-type motion. Line scans were acquired in the zig-zag scan direction (i.e., meander pattern) using a step/acquisition scheme where successive lines along X and Y were shifted by 5 μm and 25 μm, respectively. The scan rate was 30 μm s^{-1}. Two types of Al/Cu samples were used, with the Al and Cu metals either in direct physical contact or physically separated, as described above (Fig. S2). In the latter case, the separation between the two metals was sufficient to

prevent any eventual product formed on one metal from altering the local chemistry of the other. For these samples, the electrical coupling of the two metals was established with metal wires protruding at the back of the epoxy resin. Inhibitory films were prepared *ex situ* with regards to the Pt tip, that is, after removal of the Pt tip from the measurement cell. This procedure was adopted to avoid any potential interaction of the inhibitor molecules with the Pt probe that would modify the electrochemical response of the probe. Then, the inhibitor treatment on the Al/Cu surface facing upwards in the measuring cell was carried out by pouring a solution containing the chloride electrolyte and the corresponding inhibitor. The in situ SECM measurements were performed with the Pt tip immersed in an inhibitor-free solution, and the test electrolytes were 0.5 mM FcMeOH + 0.1 M $NaClO_4$ for the feedback measurements and 50 mM NaCl for the measurements carried out in the SG/TC and redox-competition modes.

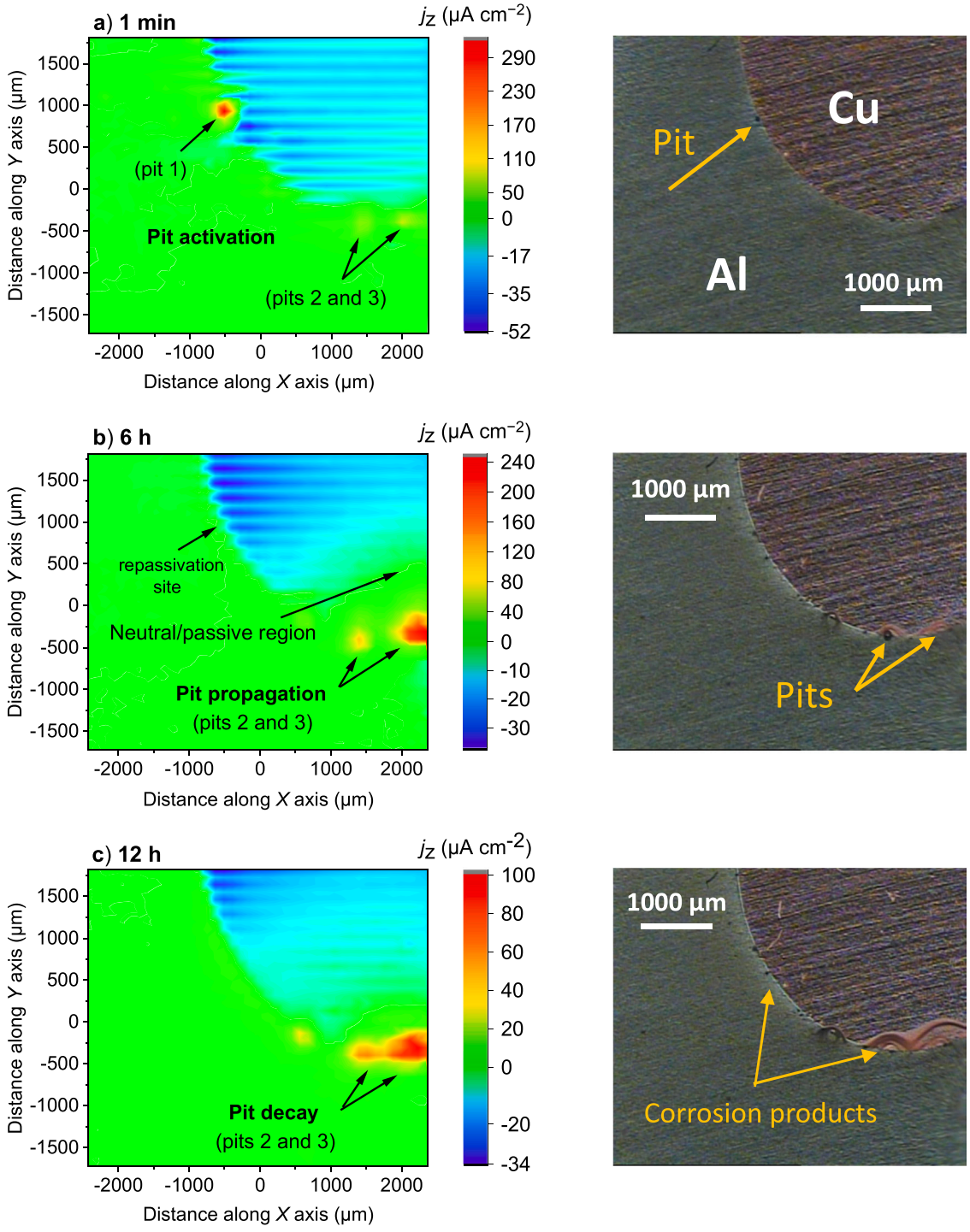

Fig. 1. SVET maps (left) recorded on an aluminum-copper galvanic couple immersed in 10 mM NaCl, and optical micrographs (right) taken just before the corresponding SVET measurements. The recording of the maps was initiated after: (a) 1 min, (b) 6 h and (c) 12 h immersion of the sample in the electrolyte solution.

3. Results and discussion

3.1. Visualization of local activation in the Al/Cu galvanic coupling: SVET characterization

3.1.1. The activity of Al/Cu in chloride solution

SVET analysis was performed on a specimen consisting of aluminum and copper surfaces conformed to maintain physical contact, and images were taken of areas around the boundary region between the two metals. Fig. 1 shows the ionic current distributions for physically connected Al/Cu immersed in an aerated 10 mM NaCl solution for different exposure times, i.e., 1 min, 6 h and 12 h, in the absence of inhibitor. Less concentrated solutions where selected for SVET measurements compared to SECM experiments (where 50 mM NaCl was chosen), because the sensitivity of SVET for measuring ionic current density is compromised by high electrolytic conductivity. The observed positive currents are due to the flux of Al^{3+} ions released from the aluminum surface, eventually leading to the hydrolysis of the metal and the release of hydrogen ions:

$$Al \longrightarrow Al^{3+} + 3e^- \quad (1)$$

$$Al^{3+} + 3\,H_2O \longrightarrow Al(OH)_3 + 3\,H^+ \quad (2)$$

It is found that the anodic activity in the aluminum sample is not evenly distributed but is localized near the copper surface, with extremely high currents, up to a maximum ionic current density of 320 μA cm^{-2}, which evidences the formation of a corrosion pit (Fig. 1a). This is not surprising since aluminum is known to be susceptible to localized corrosion attack in the presence of Cl^-, leading to the breakdown of the passive film [36–38]. The galvanic coupling of aluminum to copper leads to the relocation of cathodic activity from aluminum to copper, where it is evenly distributed over the entire metal surface. Negative ionic current densities up to − 52 μA cm^{-2}, measured at the copper surface, result from the flow of hydroxide ions generated by the reduction of dissolved oxygen, responsible for the alkalinization of the electrolyte near the reactive site:

$$O_2 + 2\,H_2O + 4e^- \longrightarrow 4OH^- \quad (3)$$

Interestingly, a near-neutral behavior was observed on the cathodically activated copper within the Al/Cu interface very close to the anodic activity (Fig. 1b and c), which can be attributed to the compensation of the cathodic ionic current density due to Al^{3+} cations departing from the aluminum surface (reaction 1) as a result of the dissolution reaction within the pits and their subsequent diffusion into the electrolyte. Furthermore, the observation of cathodic activity can be blocked or significantly hindered by the consumption of OH^- species due to coupled metal hydrolysis (i.e., reaction 2), as shown in the optical micrographs in Fig. 1b and c. The evolution of electrochemical activity with the time of exposure in the chloride solution, as monitored by the successive ionic current maps in Fig. 1, reveals that local anodic sites dynamically change location or disappear with immersion time. This can be explained by two hypotheses: (i) the repassivation of existing pits and the initiation of new pits can occur (cf. Fig. 1a and b, as well as Fig. S4a and b in the Supplementary material), and (ii) the surface can be progressively blocked by the precititation of corrosion products due to the proximity of the cathodic region. More corrosion products were deposited at the interface between the metals Al and Cu after 12 h of immersion in the chloride solution than in earlier stages of the corrosion process, i.e. after 1 min and 6 h of immersion (cf. Fig. 1), indicating the progression of corrosion over time.

Generally, pitting corrosion occurs in a series of consecutive steps [38]. After the nucleation stage, the pit can either immediately repassivate, or it can propagate further. The propagation of a corrosion pit requires the accumulation of an aggressive environment inside the pit, i.e., a local saturation with aluminum chloride; otherwise, repassivation occurs. If the current is high enough and/or the site is sufficiently occluded (less open pit sites), the pit can grow for a longer period, and this stage is called metastable pit growth. The metastable pit propagates under a diffusion-controlled process. The electrode reaction in the mass transport limited region is assumed to be:

$$Al(s) + 3Cl^-\,(aq) \longrightarrow AlCl_3(s) + 3e^- \quad (4)$$

thereafter forming a layer of anhydrous $AlCl_3$ salt that covers the metal [39]. Aluminum chloride dissolves at the salt/electrolyte interface, and aluminum ions are then transported into the bulk solution.

The SVET is not effective in distinguishing pitting stages, but it provides valuable information on activation-passivation phenomena that occur on longer time scales, visible on successive maps. Scanning electrochemical microscopy is more suitable for the detection of nucleation and metastable stages due to the small distance between the tip and the hot spot on the substrate surface [40]. To be correctly detected by SVET, a pit must remain active for a period longer than the time taken for an individual SVET scan (here around 30 min). This implies that all anodic pitting visible in Fig. 1 is stable, since metastable pitting events for AA2024 are typically much shorter than 60 s [41]. Pit 1 seems to repassivate relatively quickly, as it was not detected during the following scan obtained after 30 min of immersion (Fig. S4a). Furthermore, we suggest that pits 2 and 3 in Fig. 1a propagate over time, which can be deduced from the pits 2 and 3 of Fig. S4a, b and of Fig. 1b, where the pit current densities and sizes are much higher than in Fig. 1a. In addition, a decrease in the rate of stable pitting (the pits 2 and 3) with exposure time (after 12 h of immersion) was observed in Fig. 1c.

Another characteristic of pitting corrosion herein observed was the evolution of gas bubbles from anodically active corrosion sites (i.e., the pitting sites) at the Al/Cu interface (see Video 1), which are attributed to hydrogen evolution following electroreduction of hydrogen ions:

Supplementary material related to this article can be found online at doi:10.1016/j.corsci.2023.111114.

Such a cathodic process has been reported to evolve from anodically activated sites in AA2xxx aluminum-based alloys, giving rise to discontinuous corrosion and severe localized corrosion (SLC) phenomena [4–6]. This behavior has been associated primarily, but not exclusively, with the presence of T1 phase particles, involving lithium dealloying, copper enrichment, detachment and reprecipitation phenomena. Hydrolysis (reaction 2) and hindered diffusion at the mouth of (partially) covered pits are known to promote local acidification, thus initiating reaction (5), with attack progressing at grain boundaries accompanied by reprecipitation of T1 phase components (such as copper) in those alloys. Although the mechanism has not yet been fully revealed, it appears that, interestingly, at locations where the naturally occurring layer of aluminum oxide has been locally depassivated (i.e., at the active anodic site), there is a sufficient overvoltage for the evolution of hydrogen (cathodic process) due to the large difference between the reversible potentials for aluminum oxidation and hydrogen evolution [42]. This fits well with the trend observed here for pure aluminum to behave as a sacrificial anode, with no exposed intermetallic particles. The fact that, despite the cathodic activity being supported by the large copper surface, the bubbles form precisely at the boundary suggest that the hydrolysis and local acidification at the locations where the Al^{3+} and OH^- ions from reactions (1) and (3) get together plays a major role in surface activation and hydrogen evolution during aluminum dissolution. This phenomenon will be elaborated in more detail in the Section 2.2.

$$2\,H^+ + 2e^- \longrightarrow H_2\uparrow \quad (5)$$

As a consequence, ionic current densities and pit sizes may be erroneous due to underestimation of the true anodic pit current due to H_2 evolution inside the pits; $j_{net} = j_a - |j_{H_2}|$. In the literature, it was reported that the true anodic pit current could be 15–20 % larger than the measured anodic pit current [39,43,44]. The cathodic currents

corresponding to hydrogen evolution are masked by larger anodic currents resulting from the oxidation of aluminum. That is the main limitation of SVET, along with the inability to identify the species causing the ionic flow.

3.1.2. Corrosion inhibition of the Al/Cu system in MBI-containing solution

The electrochemical activity of Al/Cu was significantly reduced when the copper surface was treated with the MBI inhibitor, as shown by the ionic current density range shown in Fig. 2a and b. At the early stage of corrosion inhibition, i.e. after 1 min of immersion in a solution of 1 mM MBI + 10 mM NaCl (with inhibitor reservoir), both the anodic and cathodic reactions were suppressed, supporting that the MBI inhibitor was (almost) instantly effective (see Fig. 2a, and Fig. S5a in the Supplementary material). Moreover, no pitting was observed, with the anodic ionic currents being homogeneously distributed with values close to the background noise. For copper, the MBI molecule has been shown to exhibit high corrosion inhibition efficiency in near-neutral chloride solutions [12,15,16,35,45–47], acting as a mixed-type inhibitor (anodic and cathodic), with a stronger anodic effect, while the thiol/thione group does not adsorb on Al surfaces [7]. Thereafter, a thin layer is believed to develop on the copper, partially isolating its active sites from the environment, thereby preventing the cathodic reaction and, consequently, the sacrificial anodic dissolution in the galvanic system. Under such circumstances, it was expected that the copper surface would become so effectively blocked by the thicker Cu-MBI layer that the cathodic reaction should take place quantitatively on the aluminum surface along with the anodic sites. However, the strong driving force favored that the weak electrochemical activity was mostly distributed by exhibiting anodic behavior on Al, while some unblocked sites on copper still sustained localized cathodic activity up to -10 μA cm^{-2} (Fig. 2a). After 24 h immersion in the chloride solution containing MBI (Fig. 2b, S5b), the cathodic activity on the copper was rather homogeneously distributed, although still limited to -6 μA cm^{-2}, while most of the aluminum surface remained passive except for a localized anode at the boundary between the two metals, that exhibited a maximum ionic flux of 1.6 μA cm^{-2}. From inspection of the corresponding optical image (shown in Fig. S5b in the Supplementary material), it is likely that the growth of corrosion products in this area promotes local acidification, which could increase the aggressiveness of the environment after prolonged exposure, leading to local anodic activation.

Organic inhibitors usually provide limited protection in situ and even less after the metal substrate is removed from the solution containing the inhibitor. Therefore, after 24 h of in situ measurements in the MBI reservoir, the cell was quickly washed with distilled water to remove traces of inhibitor and then filled with a 10 mM NaCl solution to determine the effectiveness against corrosion in a chloride environment containing no MBI reservoir. At the early stage of immersion in a chloride-containing solution, i.e., after 1 min of immersion (Fig. 2c, S5c), the ionic current density range increased compared to the solution containing MBI (Fig. 2b). However, the ionic current densities were significantly lower than in the case of the blank sample (Fig. 1). With time exposure to the chloride solution, i.e., after 12 h of immersion (Fig. 2d, S5d), the currents remained low, indicating moderate retention of inhibitory properties. Notably, no pit formation was observed to progress into the propagation stage even after 12 h immersion in 10 mM NaCl.

3.1.3. Corrosion inhibition of Al/Cu system in OPA-containing solution

When the Al/Cu pair was treated with OPA (see Fig. 3a and b), the

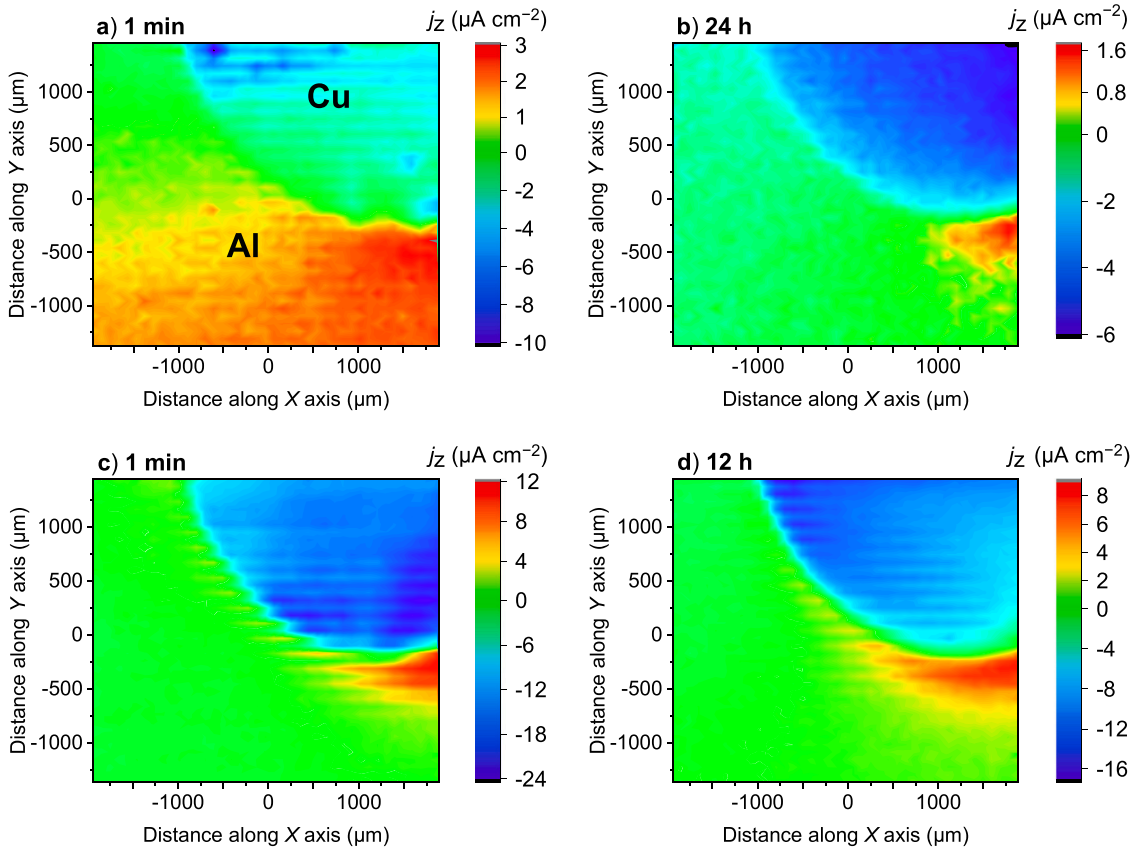

Fig. 2. SVET maps recorded on an aluminum-copper galvanic couple during its immersion in (a,b) 1 mM MBI + 10 mM NaCl at selected exposure times: (a) 1 min and (b) 24 h. Subsequently, the inhibitor-containing solution was replaced with 10 mM NaCl and SVET maps were recorded after (c) 1 min and (d) 12 h in the inhibitor-free solution.

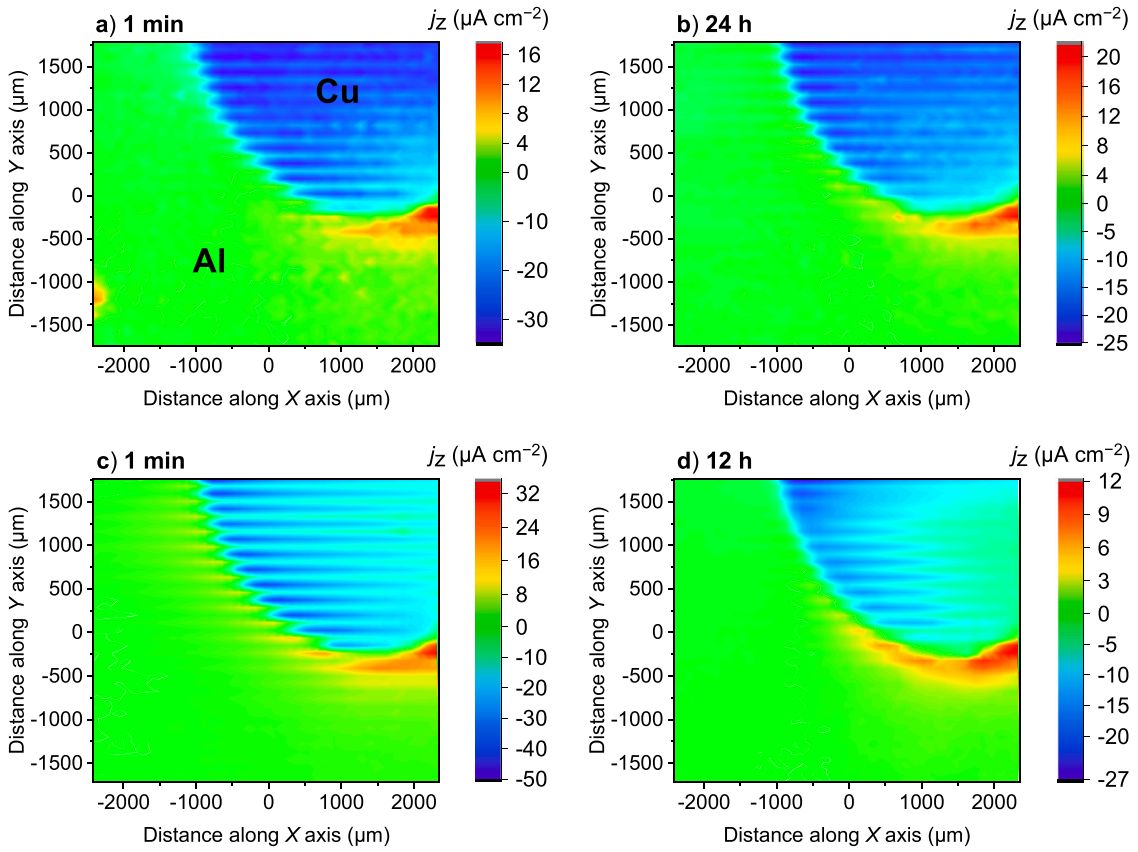

Fig. 3. SVET maps recorded on an aluminum-copper galvanic couple during its immersion in (a,b) 1 mM OPA + 10 mM NaCl at selected exposure times: (a) 1 min and (b) 24 h. Subsequently, the inhibitor-containing solution was replaced with 10 mM NaCl and SVET maps were recorded after (c) 1 min and (d) 12 h in the inhibitor-free solution.

ionic current densities decreased compared to the untreated sample (blank) (cf. Fig. 1), but not as significantly as in the case of the treatment with MBI (Fig. 2). First, after 1 min immersion in 1 mM OPA + 10 mM NaCl solution, the full range of ionic current density extended from − 34.6 μA cm^{-2} to 17.4 μA cm^{-2} (Fig. 3a, S6a), then fairly localized anodic currents after 24 h immersion increased to 21.6 μA cm^{-2}, but with no trace of pitting, while the cathodic currents slightly increased to − 25 μA cm^{-2} (Fig. 3b, S6b). These rather higher cathodic current densities, compared to the MBI treatment, can be explained by the fact that OPA does not have any inhibitory properties against Cu corrosion [15]. Therefore, the copper surface can still expose active sites where oxygen can be reduced (reaction 3), which demands electrons from the aluminum surface. However, OPA is recognized as a satisfactory inhibitor for Al [7–9,48], which prevents the oxidation of aluminum, leading to the fact that no pitting of Al was observed. However, the driving force resulted in significant anodic ionic currents recorded at the Al side of the Al/Cu interface, revealing limited inhibitory efficiency under galvanic connection.

Fig. 3c and d show the ionic current density distribution recorded over the Al/Cu sample after replacing the OPA solution (inhibitor reservoir) with 10 mM NaCl (without inhibitor reservoir), following the same procedure employed above in the case of the experiments with MBI. After 1 min of immersion (Fig. 3c, S6c), the range of ionic current densities increased significantly compared to the OPA-containing solution (Fig. 3b), while cathodic currents were comparable to the untreated system (blank) (Fig. 1). Interestingly, the ionic current density range decreased significantly after 12 h of immersion in 10 mM NaCl (see Fig. 3d, S6d), with ionic currents even smaller than those observed after 24 h of immersion in the OPA reservoir solution (Fig. 3b). Indeed, no propagating pits were observed on the aluminum surface, likely due to protection by the deposition of corrosion products. The results support that MBI is a much more effective inhibitor for reducing Al/Cu corrosion than OPA. In principle, the galvanic corrosion should be limited by the cathodic reaction (i.e. ORR in a near-neutral solution) on the copper surface [23]. Given that the MBI met these expectations, it looks promising for possible application in a more complex system like the 2024 aluminum alloy.

3.2. *Chemical and surface characterization of the Al/Cu system by SECM*

A Pt microelectrode with a diameter of 10 μm was used as the SECM probe for the investigation of the Al/Cu system. The diffusion steady-state current density is governed by the mass transfer of R (i.e., reduced species) in solution to the probe (as given by the Cottrell equation, $i_{T,\infty} = 4nFDca$, where n is the number of electrons passed per mole of the reactant, F is the Faraday constant, D is the diffusion coefficient of the reactant, c is the concentration of the reactant in solution, and a is the radius of the microelectrode. Hence, the limiting current is proportional to the sensed concentration of the electroactive species, but also to the thickness of the diffusion layer [19]. The SECM probe was first characterized by performing the cyclic voltammogram shown in Fig. 4a, taken at a scan rate of 10 mV s^{-1} in 0.5 mM ferrocene-methanol (FcMeOH or abbreviated Fc) mediator + 0.1 M $NaClO_4$ electrolyte. A single voltammetric wave was observed at potentials more positive than 0.20 V, corresponding to the oxidation of ferrocene (Fc) to ferrocinium (Fc^+), i.e., effectively a Fe(II)/Fe(III) redox conversion. From inspection of the sigmoidal (S-shaped) curve, a potential equal to + 0.50 V vs. Ag/AgCl was selected to perform approach measurements while promoting the oxidation of the redox mediator under a diffusion-limited regime.

Changing the mediator concentration and/or its mobility within the diffusion layer next to the probe, as expected when approaching the

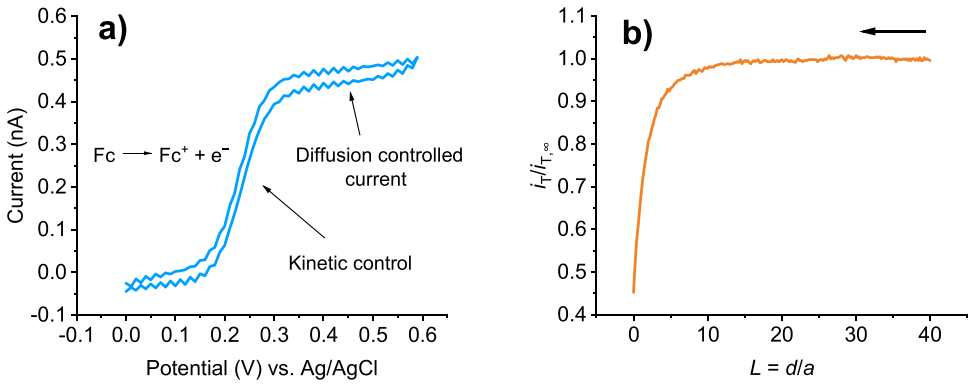

Fig. 4. (a) Cyclic voltammogram of a Pt microelectrode in a 0.5 mM ferrocene-methanol + 0.1 M $NaClO_4$ solution. Ferrocene-methanol (FcMeOH) oxidizes above ca. + 0.2 V to form the ferrocenium ion (Fc^+). The diffusion limiting current measured was 0.48 nA. (b) Approach curve measured at the SECM-tip biased at + 0.50 V in 0.5 mM FcMeOH + 0.1 M $NaClO_4$ solution. The curve was recorded by placing the tip over the resin surface to obtain the characteristic negative feedback effect. This curve is given in dimensionless form by plotting $I_T = i_T/i_{T,\infty}$ (i.e., the tip current normalized by the current far from the substrate) as a function of $L = d/a$ (the tip–substrate distance normalized by the tip radius). The arrow indicates the direction of movement of the microelectrode.

surface of the substrate, enables to determine the position of the sample (along the *Z* axis) from the Pt tip [49]. For this purpose, the faradaic current is monitored as the biased Pt tip approaches (moves in the *Z* direction) towards the surface (Fig. 4b). Once the Pt tip reaches distances very close to the sample surface, the diffusion of Fc is hindered, and the currents recorded by the tip will vary greatly from the steady diffusion-limited current, depending on whether the sample is an insulator or a conductor, as well as its tendency towards charge transfer. As represented in Fig. 5, when the substrate is insulating or any other hindrance to fast electron exchange occurs (such as an efficient passive.

layer or inhibitor film), the diffusion of R (Fc) to the tip will be partially blocked, and therefore smaller feedback currents will be measured as the tip approaches the substrate (i.e. negative feedback in Fig. 5a and b). On the other hand, in the case of a conductive substrate which also presents adequate physicochemical characteristics (namely surface potential and fast electron transfer kinetics), the oxidized form O (Fc^+), formed at the tip, can be reduced (i.e. regenerated) at the substrate, producing R (Fc), which diffuses back to the tip. Consequently, i_T becomes larger than when the tip is far away ($d \longrightarrow \infty$) from the substrate, i.e. $i_T > i_{T,\infty}$. This increase in current is called positive feedback (Fig. 5a and c) [17–19]. In both cases, the smaller *d*, the greater the "feedback" effect on the current. Thus, the ratio $i_T/i_{T,\infty}$ can be used as a measure of the distance, *d*, between the tip and the substrate and as an indicator of the nature (insulating or conducting) of the sample [50]. In this work, approach curves were always recorded over the resin substrate in the sample, thus effectively recording a negative feedback behavior. To prevent the tip from touching the surface, the approach curve was controlled by stopping the microelectrode when the measured current was reduced to half of the limiting current in the bulk electrolyte. In this way, the electrode was located in close proximity to the sample. After setting the tip-substrate distance to about 10 μm, all remaining experiments were performed while keeping the *Z*-position constant, also while scanning the Al/Cu sample along the *X* and *Y* axes to obtain maps of the surface.

3.2.1. *Local corrosion in the Al/Cu system in physical contact*

In situ localized electrochemical reactivity of the Al/Cu surface in 50 mM NaCl solution at free corrosion potential was monitored by SECM under amperometric operation. First, SECM was used in the substrate generation-tip collection (SG/TC) mode to image active sites on the surface of Al galvanically and physically coupled to copper. In this case, the platinum (Pt) tip oxidizes the H_2 evolving from the corroding surface

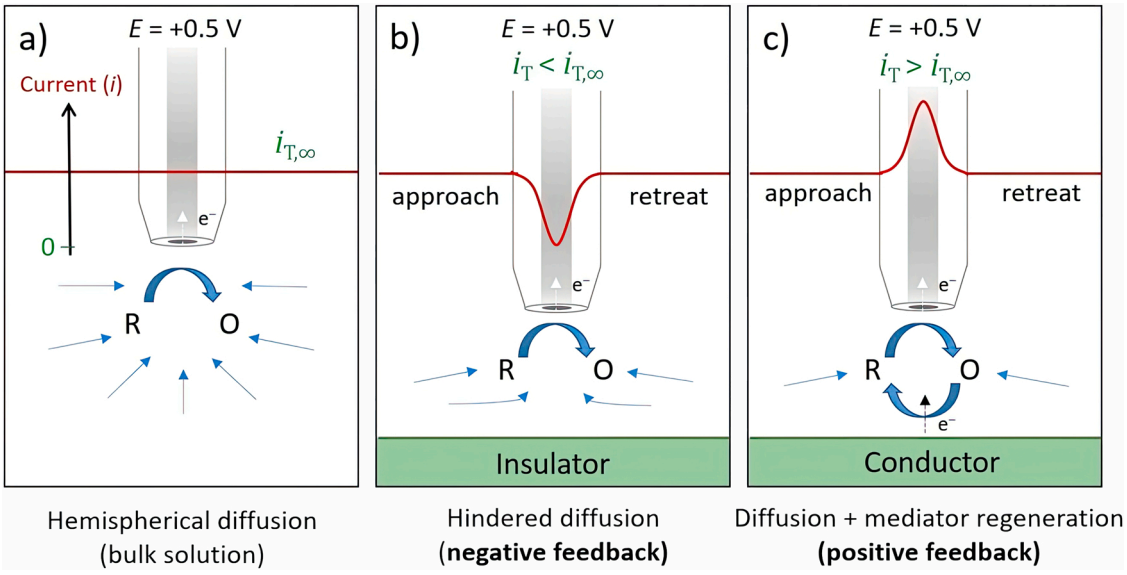

Fig. 5. Basic principles of scanning electrochemical microscopy (SECM) operating in the feedback mode: (a) when the tip is located far from the substrate, diffusion leads to the measurement of steady-state current at the tip, $i_{T,\infty}$; (b) when the tip is placed in the vicinity of an insulating substrate, hindered diffusion leads to the measurement of a tip current $i_T < i_{T,\infty}$; (c) when the tip is placed in the vicinity of a conductive substrate, the combination of mediator diffusion and regeneration leads to $i_T > i_{T,\infty}$. The current transients included in (b,c) show the current measured at the tip during its approach to the surface (approach stage) followed by subsequent retrieval (retreat stage) after reaching a minimum tip-substrate distance to avoid physical contact with the substrate.

when biased at 0.0 V (Fig. 6a) [51,52]. The corresponding SECM map shown in Fig. 7a evidences the local detection of molecular hydrogen generated on the aluminum surface due to electrochemical activity (i.e., the corrosion process), and the tip currents related to this process show a maximum value that reaches 0.43 nA. This verifies the occurrence of autocatalytic pitting corrosion of Al by the accumulation of hydrogen ions in the vicinity of the pits, which is believed to be caused by the presence of a depassivating environment (containing chloride) which induces local rupture of the oxide film [36–38]. It is interesting to note the existence of "extended current signals" belonging to the evolution of hydrogen gas, which is due to convective effects resulting from the movement of the electrolyte produced by the scanning tip. To avoid such an effect, line scans should be performed at slower scan rates, thus at the expense of longer scan times in terms of scan size, but this choice depends on which information is of utmost importance. As a compromise condition, a scan rate of 30 μm s^{-1} was applied to be able to detect localized hydrogen generation and attribute the maximum signal to the position of the evolving pit before eventual repassivation.

In addition to hydrogen detection, another cathodic reaction, the reduction of dissolved oxygen in solution, was also monitored over the Al/Cu sample in the same solution used in the previous measurement. To this end, redox-competition (RC) measurements, in which the Pt tip and the substrate compete for reacting with the same analyte (O_2 in this case), were performed at a tip potential of − 0.70 V to yield the ORR (Fig. 6b). The SECM map, obtained after 1 h of immersion in a 50 mM NaCl solution (Fig. 7b), shows two distinct regions. Very low current values (close to zero) were evenly distributed over the copper metal as expected in the Al/Cu galvanic system, where copper represents the cathodically active surface. Oxygen consumption occurs on the Cu surface, and therefore less oxygen is available for electroreduction at the tip. Considering the weak oxygen currents detected throughout the whole area, affected at least by oxygen diffusion hindrance in addition to the competition effect (Fig. 6b), a minimal effect can alter the tip current at certain places leading to the measurement of artifacts in the line scans. The movement of the electrolyte, which results from the movement of the tip, can contribute to the spread of current signals and, thus additional interference. Also, since Al is in physical contact with Cu, the electrochemical reactions can become entangled in the electrolyte.

Scanning was continued alternately and consecutively, with SG/TC mode applied after 2 h (Figs. 7c) and 4 h (Fig. 7e) of immersion, whereas redox-competition mode after 3 h (Figs. 7d) and 5 h (Fig. 7f) of immersion. Successive current maps for hydrogen detection showed a very small stationary tip current when scanning the entire Al/Cu surface with no evidence of pitting corrosion. This reveals that the pits have become repassivated over time, as previously demonstrated using SVET. On the other hand, successive current maps for oxygen reduction revealed that the currents measured above the copper after 5 h of immersion were close to zero, which was attributed to prolonged corrosion, i.e., to the cathodic consumption of oxygen on copper. This correlates well with the SVET observations in Fig. 1, where copper maintained the cathodic activity throughout the whole experimental series at the expense of a few pits distributed along the aluminum surface (eventually not detected in the selected area scan) or homogeneous mild anodic activity barely distinguishable in the SVET maps previously discussed. Also, it is important to note that the boundary between the two metals became more evident with immersion time from inspection of the RC-SECM images (cf. Figs. 7b, 7d and 7f).

These first SECM measurements reflect one series of experiments that depict a fairly homogeneous behavior of the system during degradation. However, minute changes in surface conditions appeared to alter the system response from smoothly evolving to locally exhibiting vivid degradation. In a set of the latter measurements performed in redox-competition mode (Fig. 8a) during the early stages of corrosion, some unexpected features were observed. Immediately after immersion in 0.5 M NaCl, homogeneously distributed small cathodic currents (i.e., currents close to zero) were detected over most of the Al/Cu surface, which correlates well with the observation reported in Fig. 7b. However, some 'hot spots' have also been found to exhibit higher currents (i.e., more negative currents reflecting greater local oxygen availability). A possible interpretation may relate to a certain local electrochemical activity or to evidence topographical information on the evolution of the corroding Al surface. On the other hand, HER is thermodynamically possible in an aqueous environment at the free corrosion potentials for aluminum, with HER rates increasing with anodic polarization despite the low HER catalytic activity of Al and the predictions of conventional electrochemistry, a phenomenon reported as "negative difference effect", or "anomalous or anodic" hydrogen evolution [42,43,53–56]. The same scenario was observed during free corrosion by galvanic coupling with copper (cathodically active region), mimicking the effect of intermetallics [42,55]. Given this, it was hypothesized that the local increase in current signals seen in Fig. 8a, associated with oxygen availability, can be attributed either to interference with anodic hydrogen evolution (although this was not observed in previous experiments shown in Fig. 7 that were apparently less active), or to indentations in a surface due to localized metal dissolution that favors the diffusion of oxygen towards the tip.

In order to correlate this greater oxygen content and the presence of active pits, mapping in RC mode (Fig. 8a) was followed by alternating

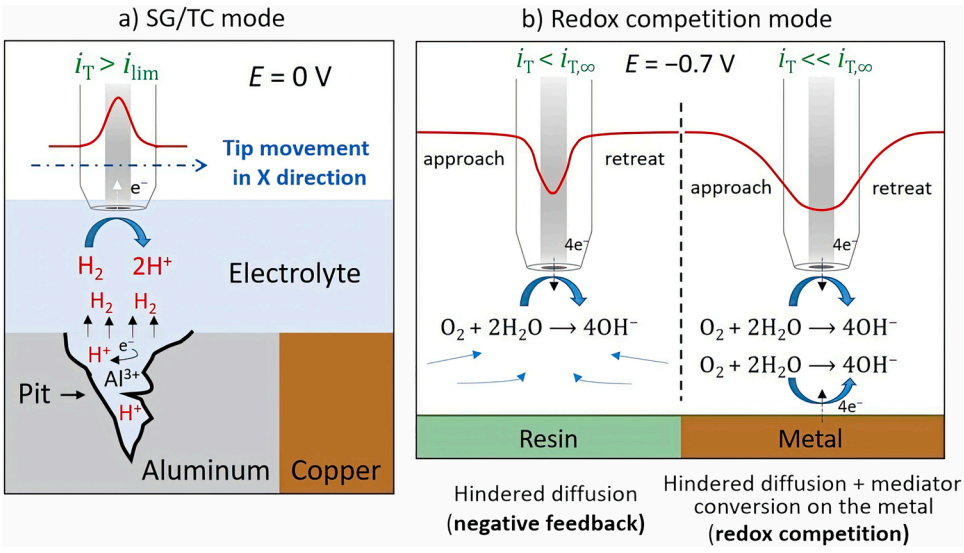

Fig. 6. Basic principles of scanning electrochemical microscopy (SECM) operated in other amperometric operation modes employed in this work: (a) substrate generation-tip collection (SG/TC) for the detection of hydrogen evolution at the Pt probe, and (b) redox-competition, which is based on the competition between the metal and the Pt tip for the electroreduction of the molecular oxygen dissolved in the solution. As a redox mediator naturally present in solution while measuring oxygen in (b), in the absence of competition effect the probe currents are also expected to decrease at a lower extent due to diffusion hindrance (negative feedback).

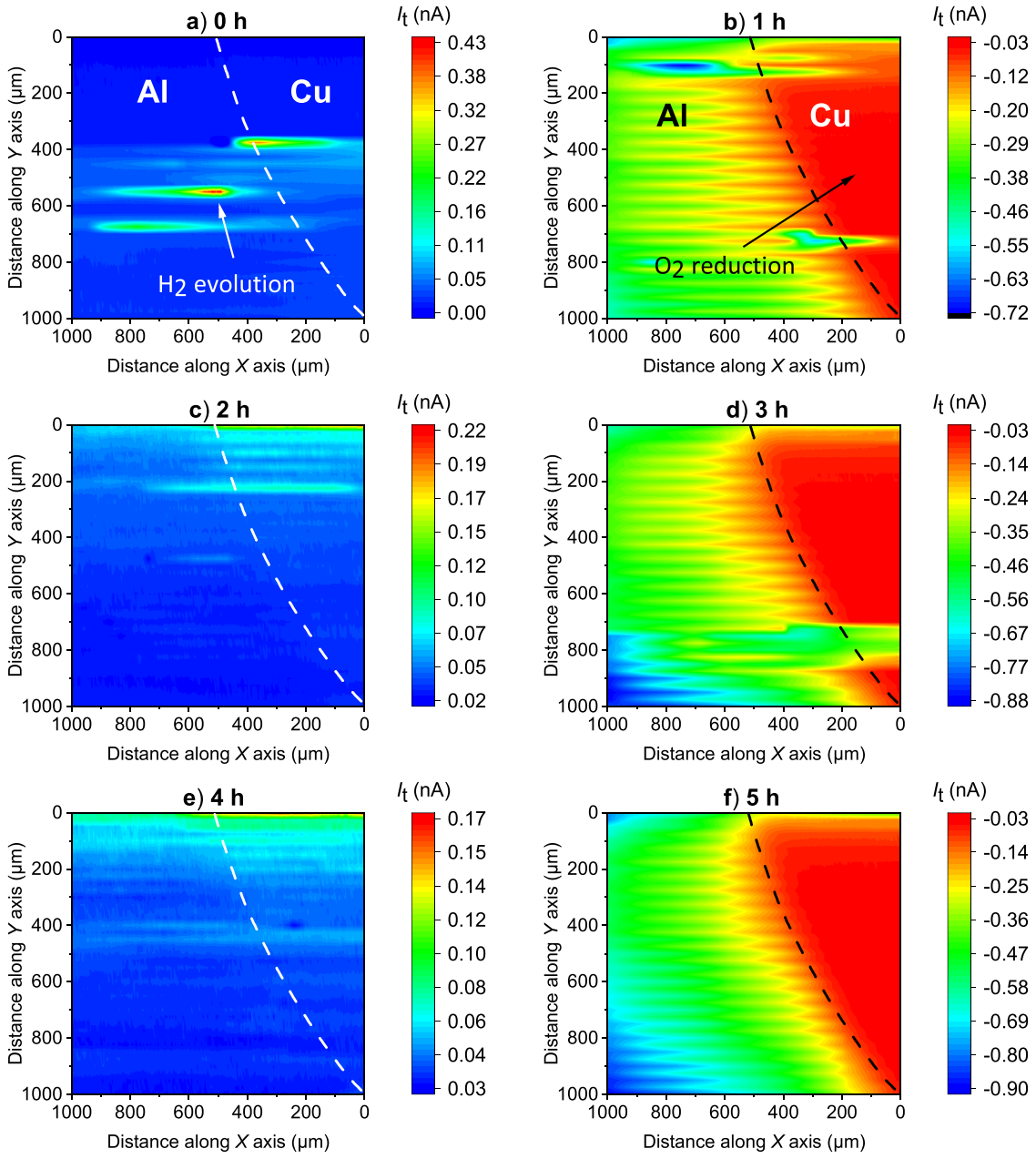

Fig. 7. Consecutive maps recorded on the physically- and electrically-coupled Al/Cu system immersed in 50 mM NaCl solution during 5 h under open-circuit potential (OCP) condition. They were obtained alternately using two different SECM operation modes: in substrate generation-tip collection (SG/TC) mode with tip potential set at 0.0 V vs. Ag/AgCl, KCl (sat.) after (a) 0 h, (c) 2 h, and (e) 4 h of immersion; and in redox-competition mode with tip polarized at − 0.7 V vs. Ag/AgCl, KCl (sat.) after (b) 1 h, (d) 3 h and (f) 5 h of immersion. The scanning rate of the tip was chosen as a compromise between the dimension of the scanned area and the time allowed for acquiring a single image frame. Tip diameter: 10 μm. Tip-substrate distance: 10 μm. Scanned area: 1000 μm × 1000 μm. Scan rate: 30 μm s^{-1}.

SG/TC mode mapping in the same electrolyte, where the currents originating from H_2 oxidation were detected by the Pt tip. The corresponding SECM profile of Fig. 8b shows hydrogen currents from localized highly active sites (pits) with faradaic currents up to 2 nA. Furthermore, it was observed that some signals originating from O_2 electroreduction and H_2 oxidation almost overlap, as shown in Fig. 8c and d (extracted insert from Fig. 8a and b, respectively). It should be emphasized that this is not the real shape of the signals, as they were built here on an image with a ratio of 50 μm × 1000 μm. The actual image size is shown in Figs. S7 and S8, where the signals are quite elongated.

To determine whether the 'hot spot' represents a reduction in local cathodic activity, the existence of an attacked site or interference, the first three line scans interpolated to form the SECM image in Fig. 8c) were extracted as shown in Fig. 8e. All line scans for oxygen reduction show noisy fluctuations between $Y = 0$ and 50 μm in the initial recording period over a distance along the X-axis from 800 to 1000 μm, after which the tip current decreases (i.e. it reaches less negative values) due to competitive reaction between sample and tip (i.e. the ORR activity increases in/near the pit). One signal from the ORR fluctuation at $Y = 0$ μm is consistent with the current corresponding to H_2 oxidation at $Y = 0$ μm, which then decreases sharply to reach a plateau (Fig. 8f). Interestingly, the line scan recorded in RC mode at $Y = 25$ μm (Fig. 8e) shows a high current transient spanning 200 μm, i.e., from $X = 600$–800 μm, which correlates with the initial and maximum current corresponding to H_2 oxidation (Fig. 8 f, line scan at $Y = 25$ μm). At sites where hydrogen evolves (i.e., the cathodic reaction within the local anodes in Fig. 8d), the Pt tip experienced high cathodic currents

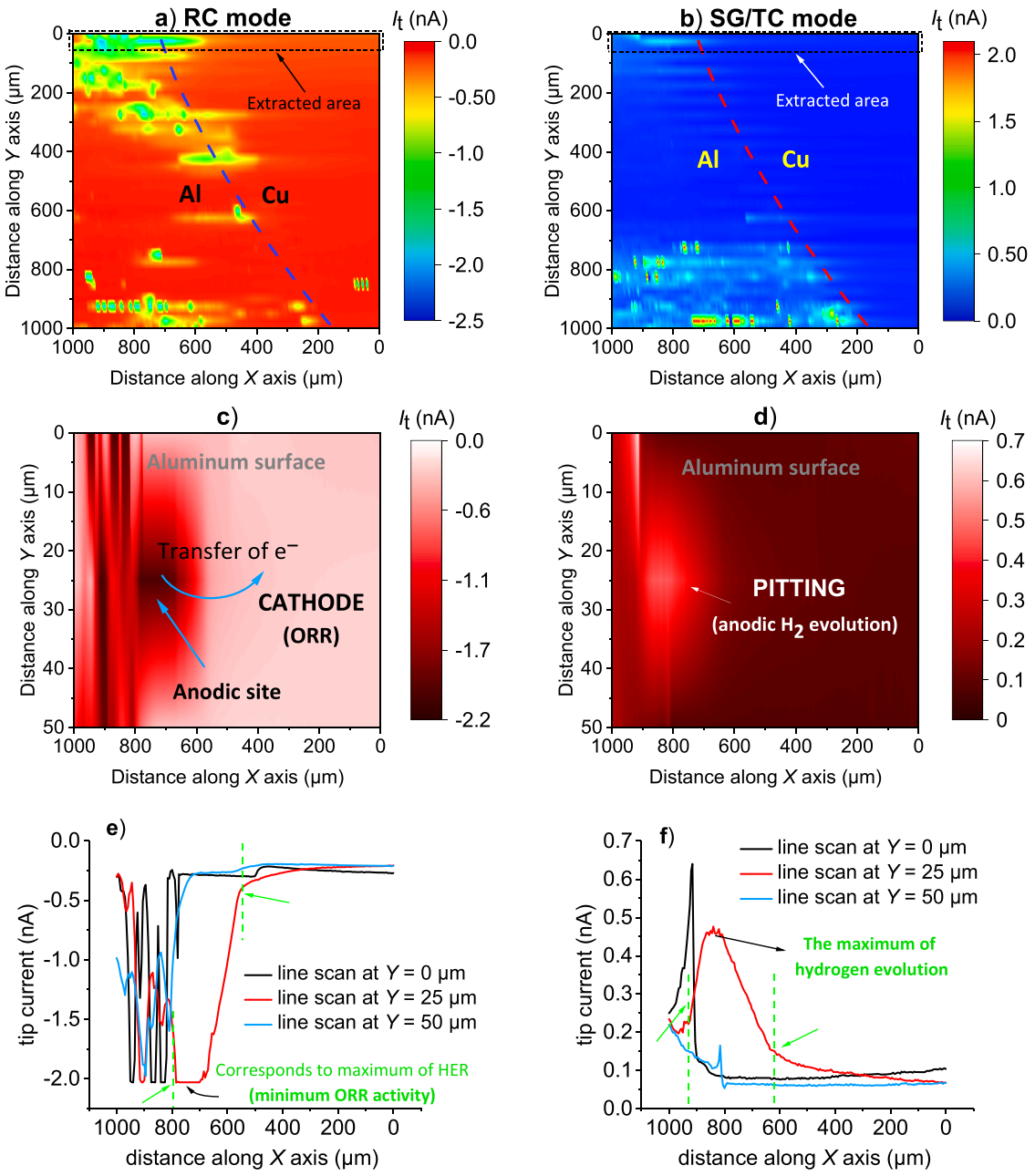

Fig. 8. SECM images recorded on physically and electrically coupled Al/Cu system immersed in 50 mM NaCl solution under OCP conditions. They were obtained in: (a) redox competition mode after 1 min of immersion and (b) SG/TC mode after 33 min of immersion in 50 mM NaCl solution at OCP. Images (c) and (d) represent the magnification of the upper side from maps (a) and (b), respectively. Tip diameter: 10 µm. Tip-substrate distance: 10 µm. Scan rate: 30 µm s^{-1}. Increment of *X*-line: 5 µm. Increment of *Y*-line: 25 µm. Line scan direction: from left to right. Graphs (e) and (f) show the three line scans extracted from the interpolated images (c) and (d), respectively.

associated with oxygen reduction (i.e., the remaining oxygen concentration in the electrolyte that was not consumed at the cathodic sites on the surface of the substrate; see Fig. 8c); however, increased ORR activity on the metal surface is noted only in the immediate vicinity of the anodic sites.

A schematic illustration of the apparent surface activities during the scan acquisition is provided in Fig. 9. According to our observations, as hydrogen evolution decreases, aluminum again becomes competitive with the Pt probe for oxygen reduction. The shape of the redox regions in Fig. 9 is based on the behavior of the line scans of Fig. 8e and f. At this stage, it could be questioned why not all the signals from the RC mode (Fig. 8a) correspond exactly to the signals obtained in the SG/TC mode (Fig. 8b). A reasonable justification would be developed on various features, namely the nature of pitting is metastable (i.e., the time difference between the consecutive scans is 1 h) and convection cannot be completely neglected, not only due to insufficiently slow scanning but also due to the formation of H_2 bubbles on the surface which pushes the electrolyte away in a radial direction. Therefore, the microelectrode can be blocked (partially isolated) by the growth or rapid evolution of H_2 bubbles from the active sites, resulting in reduced metal activity and false signals.

We initially thought that the enhanced faradaic currents measured at the tip, when scanning over or near the indentation sites (possibly pits as observed in Fig. 8a and c) at a constant height, were due to a larger amount of soluble oxygen than became available from the volume of electrolyte inside the pit, and the sample no longer hinder the diffusion

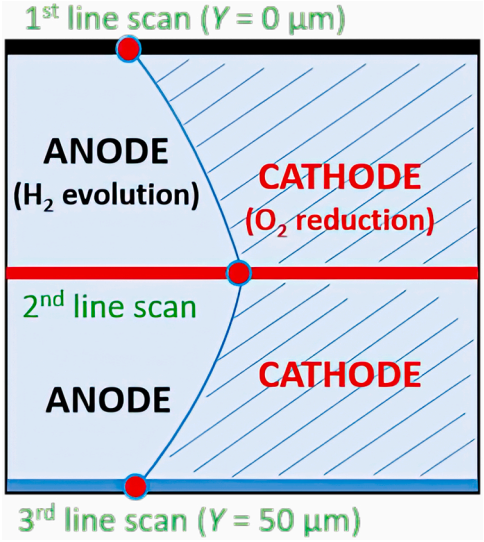

Fig. 9. Sketch describing the reconstruction of corrosion processes observed in Fig. 8c and d. The shape of the local anodic spot (i.e., corrosion pit), according to the hydrogen reduction signal, and the cathodic regions where the dissolved oxygen is reduced are based on the linear scan signals in Fig. 8e and f. The cathodic reduction of oxygen does not occur at the sites where hydrogen evolves (at the local anodes) but around the anodic sites.

of oxygen from the bulk (illustrative scheme given in Fig. 10). The indentation in the aluminum would not be a surprise given that in addition to the already existing pit, the H^+ released into the electrolyte during H_2 oxidation at the Pt tip can contribute significantly to local acidification in the vicinity of the Al surface and thereby increase metal dissolution. The voids formed could also lead to less competition for oxygen reduction between the Al surface at the bottom of the indentation and the tip (as a result, topographical information about the pit would be obtained). However, the diameter of the Pt tip is too large to address the topography within the pit, which is very small in size. Advanced modes and techniques, such as shear-force SECM and AFM-SECM [57,58] would be required to discern the effect of surface topography from surface reactivity.

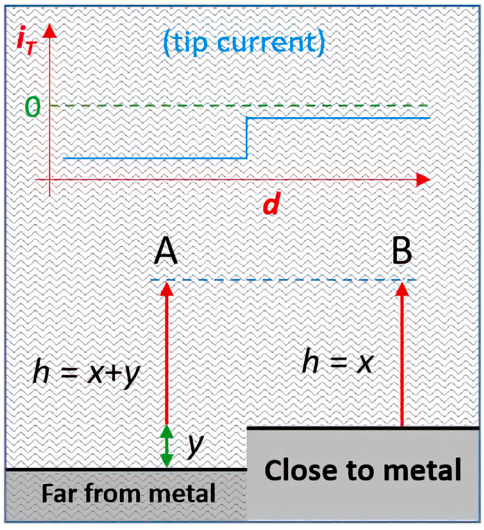

Fig. 10. Diagram illustrating the relationship between the tip current and the tip-substrate distance *d* for the line scans shown in Fig. 8c and d (as sketched in Fig. 9). A and B are the positions of the tip located far from the metal and close to the metal, respectively. The tip currents above an indentation are bigger (i.e., i_T attains more negative values) relative to imaging near the metal surface.

3.2.2. Limitations of SECM with the interconnected Al-Cu system

The effect of the inhibitors was next tested not only by their chemical effects (investigating the inhibition of ORR and/or HER reactions at the active sites) but also by taking advantage of the SECM capacity to address surface conductivity and the ability towards electron exchange. This was first achieved by SECM measurements in feedback mode using ferrocene-methanol, a redox mediator commonly used in SECM, which is monitored by its oxidation and conversion at the tip. A positive feedback effect is expected at active sites capable of converting the oxidized ferrocenium ion back to ferrocene-methanol, where the tip current is locally increased, allowing analysis of local surface conductivity and reactivity. Similar measurements were made with the assembled system making physical contact between the two metals around the Cu/Al boundary. However, some difficulties and loss of sensitivity were immediately observed (measurements not shown here), so the experiments were made using a target system where the two surfaces, Al and Cu, were physically separated, and electrical contact ensued from the rear of the mold.

When the two metals were held in electrical contact, fouling or blockage of the Pt tip was observed during the measurements in feedback mode over the copper surface, resulting in a loss of signal sensed using ferrocene-methanol as a redox mediator. This effect is shown in Fig. 11, which presents four consecutive images. For each scan, the measurement started from the upper right corner (coordinates $X = 0$, $Y = 0$), and then consecutive lines were made along the X axis at different Y positions from top to bottom as seen in the pictures. The first scan was performed by scanning the Pt tip over the Cu/resin boundary without an electrical connection being made between Cu and Al (Fig. 11a). The positive feedback effect revealed a well-defined copper surface (higher currents, red area), attributed to mediator regeneration on the conductor. After the Cu was electrically connected to the Al (Fig. 11b), the faradaic currents at the beginning of the scan (top of image) began to decrease sharply as the scan progressed to more negative Y values in consecutive lines in comparison with the first image (Fig. 11a). After a few line scans, the currents dropped to near zero, reflecting a time effect that caused tip fouling or blockage. To confirm the effect, another set of consecutive maps was made in which the metals were held electrically isolated (Fig. 11c) and next electrically connected (Fig. 11d). Similar to the currents in Fig. 11a, the currents of Fig. 11c were evenly distributed on the Cu surface, but their magnitude was smaller, indicating that the Pt tip was already "blind". When Cu and Al were reconnected, the same effect was observed as in the case of Fig. 11b, i.e. the tip became even more blocked and lost all sensitivity.

A reasonable explanation for the blocking of the Pt tip can be offered based on the Pourbaix diagram for platinum [59], from which it can be concluded that the platinum tip biased at + 0.5 V vs. Ag/AgCl, KCl (sat.), corresponding to + 0.697 V vs. the Normal Hydrogen Electrode, oxidizes to $Pt(OH)_2$ at pH values above 7.5. When copper is coupled to aluminum, the cathodic reaction occurs on the copper, with the rapid release of OH^- ions, leading to a significant increase in pH. Therefore, to avoid the blocking effect of the Pt tip above the Cu surface, we established the so-called connection-disconnection procedure, achievable only when the two metals are physically separated. First, the inhibitor solution in which the Al/Cu has been immersed for a certain time is replaced by the FcMeOH solution, and then, just before polarizing the tip in the FcMeOH solution, the electrical connection between the two metals is interrupted. In this way, we avoid a rapid increase in pH while still being able to obtain information on the conductive/insulating properties of the copper surface. Thus, both the feedback effect and chemical species could be detected using SECM before and after inhibitor treatment as described in the next section. Another alternative would be to use a less common redox mediator with a less positive operational work potential for oxidation. However, this option was beyond the scope of this work.

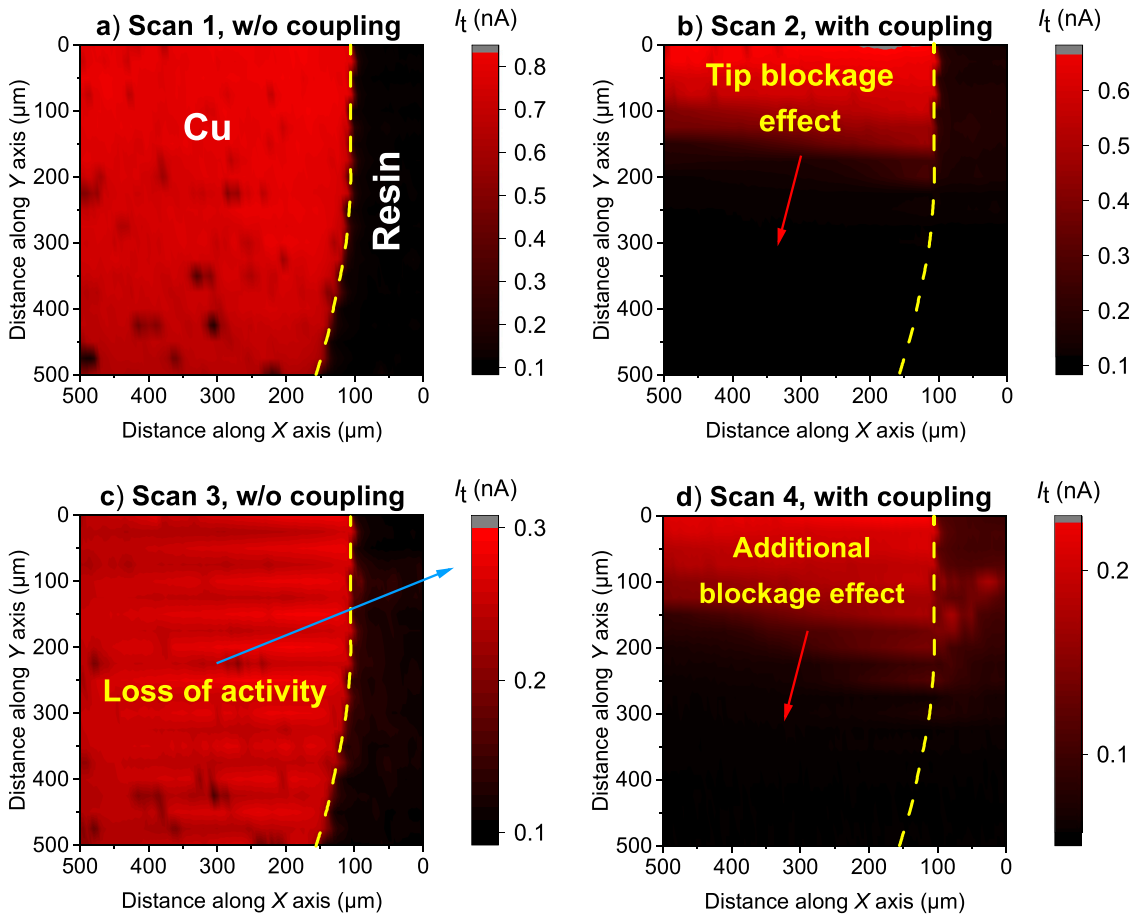

Fig. 11. Consecutive SECM images in feedback operation mode of the copper/resin boundary during immersion in 0.5 mM FcMeOH + 0.1 M $NaClO_4$ solution which exhibit the occurrence of a blockage effect of the Pt tip. Tip potential: + 0.50 V vs. Ag/AgCl, KCl (sat.). Scanned surface: copper/resin. The copper was not in electrical contact with aluminum in (a) scan 1 and (c) scan 3, but there was electrical contact between the two metals in (b) scan 2 and (d) scan 4.

3.2.3. The protection of the Al/Cu surface by MBI

In this set of experiments, the behavior of physically separated aluminum and copper was investigated prior and after treatment with MBI as the corrosion inhibitor, following an *ex situ* inhibitor treatment and the connection-disconnection strategy. Fig. 12 shows three sets of maps, each comprising three different scans over the Cu/resin covering an area of 500 µm × 500 µm, that were recorded in feedback and redox-competition modes. Scans were performed for Cu samples previously treated with or without an MBI-containing solution. It was essential to monitor the current profile only on the Cu surface because of its known interaction with MBI, which is not the case with Al [14,15].

In this manner, the Cu sample was initially scanned in feedback mode without prior MBI treatment to locate the metal and envisage its surface reactivity. Fig. 12a shows the initial 2-D measurement in the electrolyte solution consisting of 0.5 mM FcMeOH + 0.1 M $NaClO_4$ (without the addition of the aggressive chloride ions), clearly reflecting the copper (conductive) and resin (insulating) surfaces, as well as the boundary between them. After that, the test solution inside the small cell was replaced with corrosive 50 mM NaCl and the probe potential was set to − 0.70 V vs. Ag/AgCl, KCl (sat.), corresponding to the reduction of dissolved oxygen in the solution. Small currents (i.e., less negative cathodic currents) were detected above the bare copper surface (Fig. 12b), which may be correlated with partial cathodic activation favoring the consumption of oxygen according to the half-reaction (3); therefore, less oxygen is available for electroreduction at the tip. Another additional feature possibly contributing to this current decrease could be related to the fact that the grinding process for surface finishing does not produce a completely flat metal-resin interface but could result in a step due to the different hardness of copper and the resin, thus removing more material from the resin areas. As a result, the tip-to-substrate distance would be shorter when scanning on metal than on resin, and consequently, diffusion would be more hindered on copper, enhancing negative feedback. However, there is ca. 1 nA difference in Fig. 12b when the tip scans over the resin (oxygen reduction resulting in −1.4 nA tip current) and the metal (same reaction sensed at the tip with faradaic currents around −0.4 nA), which seems too big a difference for a purely negative feedback effect. Therefore, redox competition in the cathodically activated regions of copper (that was not electrically connected to the Al at this stage) must play an important role in decreasing cathodic currents even when copper self-corrodes in the absence of a galvanic connection to the more active Al surface.

On the other hand, when Cu and Al were brought into electrical contact afterwards (Fig. 12c), the map obtained in redox-competition mode showed a higher electrochemical activity manifested by an additional decrease in the faradaic currents, compared to the previous scan (Fig. 12b), when the two metals were isolated. This is evidenced by the inspection of the current values and scales, which reflect an almost zero current detected over the copper due to the complete absence of oxygen consumed on the copper surface. The increase in cathodic activity is associated with the driving force of galvanic corrosion due to the potential difference that develops between copper and aluminum, which shifted the cathodic reaction to occur exclusively on the copper surface, where it is evenly distributed over the entire surface of the metal.

When the scan of Fig. 12c was completed, the electrical connection between the two metals was still maintained, and the Pt probe was removed from the solution along the *Z* direction. In this way, the

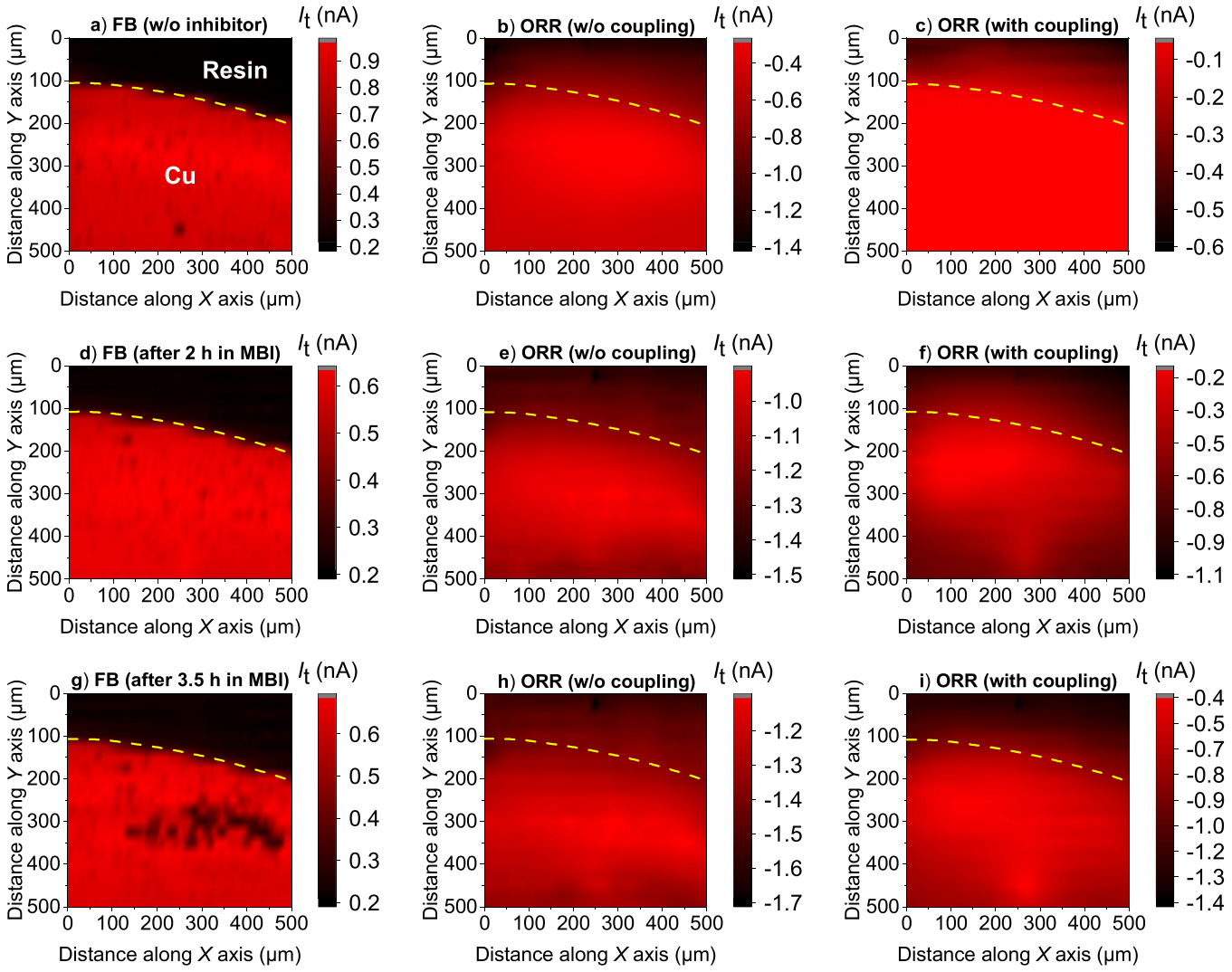

Fig. 12. SECM images showing three sets of maps, each of which includes three different scans above the Cu/resin region. Operation mode: (a,d,g) feedback mode, (b,e,h) redox-competition mode, and (c,f,i) redox-competition mode after interconnection with the Al surface. The first series corresponds to measurements performed on the model system without previous treatment with MBI (a-c). The second and third series correspond to measurements conducted after treatment in the presence of MBI for (d-f) 2 h and (g-i) with an additional 1.5 h treatment as described in the body of the manuscript. Scanned area: 500 μm × 500 μm. Tip potential and electrolyte solution for each operation mode: + 0.50 V, in 0.5 mM FcMeOH + 0.1 M $NaClO_4$ solution, in the maps recorded in the feedback mode; − 0.70 V Ag/AgCl, KCl (sat.) in 50 mM NaCl, for the maps recorded in the redox competition mode.

possibility of interaction between the surface of Pt and the MBI molecules was prevented in order to avoid any possible interaction between this inhibitor and the sensing tip [35]. The solution was then replaced with 1 mM MBI + 50 mM NaCl so that Cu was immersed in the inhibitor-containing solution for 2 h. After this *ex situ* immersion stage, the inhibitor solution was replaced with an electrolyte containing the redox mediator (namely, 0.5 mM FcMeOH + 0.1 M $NaClO_4$) and the Pt tip was introduced in the solution and moved along the *Z*-axis toward the surface until it reached the same position as in the previous measurements. In this way, all the measurements shown in Fig. 12 were performed by keeping the same *Z* position. The microelectrode was again biased at + 0.50 V to allow scanning in the feedback mode, and the electrical connection between Cu and Al was interrupted. Fig. 12d shows the SECM image recorded for the Cu sample previously treated for 2 h in a solution containing MBI. The faradaic currents detected over the Cu surface are smaller than in the scan of Fig. 12a, indicating that the Cu surface is covered by the MBI inhibitor. That is, the magnitude of the positive feedback effect is reduced because the Cu-MBI film formed on the surface of the Cu sample hinders the regeneration of FcMeOH on the substrate due to its adsorption at the active sites for electron exchange. After the scan in Fig. 12d was completed, the electrolyte solution was again replaced with 50 mM NaCl, and the probe potential was polarized at − 0.70 V to monitor the cathodic activity with the tip operating in the redox-competition mode. Fig. 12e shows increased faradaic currents (i.e., the currents were more negative) compared to the second scan in Fig. 12b, similarly measured on the Cu surface but without a protective layer of Cu-MBI. This confirms that oxygen consumption was occurring on the exposed (not connected) copper when Fig. 12b was recorded, and the decreased cathodic currents did not correlate with a pure feedback effect. Therefore, due to reduced competition between the tip and the Cu surface due to a protective layer of Cu-MBI, which effectively blocks the cathodic sites, the current values do not decay to the same extent over the conductive surface. However, when the electrical contact between Cu and Al is re-established, the galvanic coupling renders copper an active cathode again with smaller recorded cathodic currents down to − 0.2 nA as shown in Fig. 12 f. However, the redox competition effect is not only less pronounced than in the case of a previously non inhibited sample (recorded currents were close to zero in Fig. 12c), but is also more heterogeneously distributed, revealing that an inhibitory film effectively protects a large part of the metal surface through

heterogeneous adsorption resulting in areas where the cathodic process is greatly inhibited.

Finally, the third set of maps was also recorded after treatment with the MBI inhibitor. The same procedure was applied as described related to Fig. 12 d-f, including removing the Pt probe, change of electrolyte, additional immersion in 1 mM MBI + 50 mM NaCl for 1.5 h and replacement with the FcMeOH electrolyte. Fig. 12 g shows the SECM map obtained for the Cu sample after 3.5 h of immersion in a solution containing MBI. There are some areas on the Cu surface where regeneration of the redox mediator was almost completely blocked, which can be attributed to local improved insulating characteristics, that is, improved inhibitory film thickness due to a more prolonged *ex situ* exposure to an MBI-containing solution. The overall reduction in the positive feedback effect (i.e., faradaic currents become smaller after the longer inhibition treatment of 3.5 h) gave rise to an intermediate behavior between purely positive and negative feedbacks, yielding the regeneration of the mediator apparently hampered. Finally, the electrolyte solution was replaced again with 50 mM NaCl, and the probe potential was biased to − 0.70 V to monitor the consumption of dissolved oxygen over copper protected by an inhibitory layer. From the comparison of Fig. 12 h with the scans depicted in Fig. 12b and Fig. 12e, it is observed that greater currents (i.e. more negative current values) were measured above the Cu surface now, and they are associated with a reduced affinity for cathodic oxygen consumption, that is, redox competition between the tip and the copper surface is significantly impeded. When Cu was electrically coupled again to Al (Fig. 12i), the affinity for oxygen on the copper surface increased. Consequently, the corresponding currents detected at the tip were lower (i.e., less negative) than in the previous scan of Fig. 12 h that was recorded in the absence of electrical connection between the two metals. However, the reported currents were still showing comparatively higher oxygen content than in the case of Fig. 12f and Fig. 12c, which implies that the Cu-MBI film was more resistant to corrosion after 3.5 h of *ex situ* immersion, and the driving force due to the galvanic connection was effectively compensated by the presence of a cathodic inhibitor layer. Hence, the results obtained from the application of redox competition mode are consistent with those obtained in the feedback mode.

3.2.4. *The protection of the Al/Cu surface by OPA*

The set of images shown in Fig. 13 consists of a series of maps obtained for an aluminum substrate that includes galvanic coupling with copper or electrical insulation. The Al/resin boundary was measured with both metals exposed in solution and controlled electrical contact at the rear of the target. The current plots were recorded only on the Al surface because it is known from the literature [15] that OPA is a good inhibitor for Al but not for Cu. Measurements were performed on an aluminum/resin area of 500 μm × 500 μm in three different operation modes, namely feedback, substrate generation-tip collection (SG/TC) and redox-competition, with and without pretreatment with the OPA inhibitor.

First, the surface of bare aluminum (which was not electrically connected to Cu) was evaluated by biasing the Pt tip to + 0.50 V to operate under diffusion-limited conditions in the feedback mode for monitoring the regeneration of the redox mediator on the conductive substrate (Fig. 13a). Variations in the measured faradaic currents are observed, i.e. higher currents are detected above the metal surface compared to the resin, due to the regeneration of the Fc mediator on the conductive surface. Then the solution containing ferrocene-methanol was replaced with 50 mM NaCl electrolyte solution, and the tip was held at 0.0 V to measure the local concentration of hydrogen gas above the Al surface galvanically coupled to Cu, which is associated with hydrogen oxidation at the tip (Fig. 13b). No significant electrochemical activity was observed in scan 2 because the measured currents did not exceed the current value of 0.15 nA, comparable with the noise level. It was not trivial to find the hydrogen evolution spots (i.e., pitting sites) on a relatively small scanned area of aluminum, due to the stochastic nature of pitting, but a few events could be envisaged and higher current values were indeed detected over the metal, revealing hydrogen production at

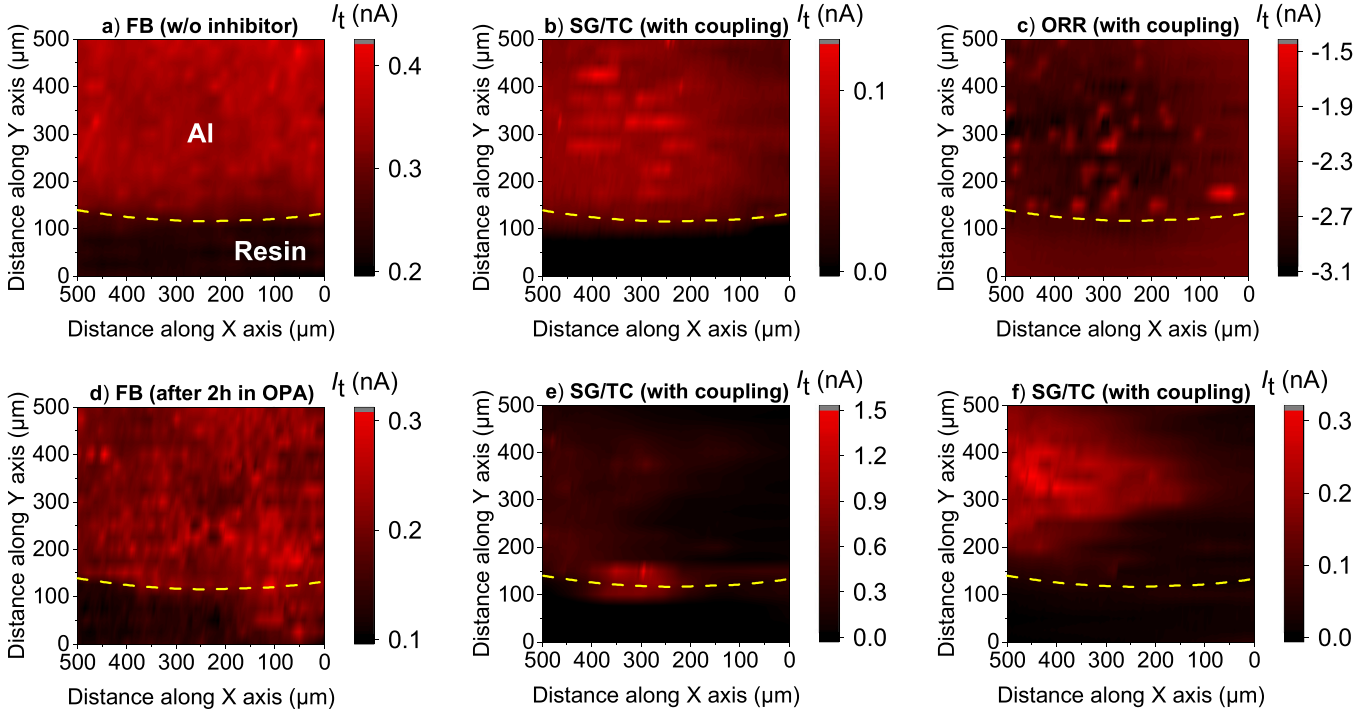

Fig. 13. SECM images showing two sets of maps, each of which includes three different scans above Al/resin region. Operation mode: (a,d) feedback mode, (b,e,f) substrate generation-tip collection (SG/TC) mode, and (c) redox-competition mode. In the first series, the bare and freely corroding Al surface was scanned in (a) feedback mode, followed by electrical connection with Cu for scanning in (b) SG/TC and (c) redox-competition modes. In the second series, Al was treated with a solution containing OPA for 2 h and measurements were performed in the feedback mode (d) without galvanic connection with the Cu metal, followed by two consecutive maps, (e) and (f) that were recorded using SG/TC while the two metals were electrically-connected.

minute locations. The tip was then biased to − 0.70 V in the same electrolyte solution to monitor cathodic activity with the Pt probe through the redox-competition mode (Fig. 13c). Since the cathodic reaction should occur exclusively on the copper surface when Al and Cu are in electrical contact, a decrease in the tip currents (originating less negative values) due to redox competition was not expected when the microelectrode was scanned above the aluminum surface. Indeed, currents as low as − 3 nA were detected over some areas of the Al surface, and those spots with apparently higher activity (i.e. smaller local oxygen current values) could be ascribed to convective phenomena under a mild bubbling regime.

Next, the Pt probe was removed from the solution along the *Z* direction, and the electrolyte solution in the small cell from the previous experiment was replaced with 1 mM OPA + 50 mM NaCl. The Al surface, electrically coupled to the copper, was exposed to the inhibitor solution for 2 h. After this *ex situ* treatment, the electrical connection between the metals was removed to reduce the potential risk of contamination of the platinum tip. The inhibitor solution was then replaced with 0.5 mM FcMeOH + 0.1 M $NaClO_4$, and the Pt tip was repositioned back at the same constant height as in the previous measurements. After setting the tip potential at + 0.5 V, the Al surface was scanned in feedback mode (Fig. 13d). Compared to the previous scan in Fig. 13a, the smaller feedback currents indicate that OPA adsorbed on the substrate and, therefore, the electron donation needed to regenerate the redox mediator was inhibited. However, the currents were not evenly distributed over the entire aluminum surface, which may be related to the lower efficiency of the octylphosphonic chain to form a dense inhibitory layer. It is well known that what determines the effective corrosion inhibition of organic molecules is their ability to form a dense organic film on the metal surface [7,60]. Next, the solution containing the mediator was replaced with 50 mM NaCl, and the tip was biased to 0.0 V to monitor the oxidation of hydrogen above the Al surface galvanically coupled to Cu (Fig. 13e). High faradaic currents, with a maximum of 1.5 nA, were detected at some locations on the Al surface near its boundary with the resin, which is associated with pitting corrosion. The OPA film probably does not provide sufficient barrier properties against the penetration of aggressive ions, such as chloride, accompanied by the driving force of the galvanic interaction. Finally, another consecutive map (Fig. 13f) recorded in SG/TC mode revealed the repassivation of the metastable pit that existed in the previous scan and a moderate localized activity at another more extended location. The maximum time difference between the detection of the metastable pit and its repassivation, as observed from the last two scans, is about 9 min since this length of time is required to record a 500 μm × 500 μm map.

The results suggest that, under galvanic connection, the bare aluminum surface corrodes homogeneously (Fig. 13b), but metastable activation results when the metal has been previously exposed to the inhibitor. Indeed, it was reported that in more aggressive solutions (namely, 3 % wt. NaCl), the presence of inhibitor would lead to a passive regime for aluminum extending from the OCP to approx. − 0.2 V vs. Ag/AgCl, KCl (sat.) [14,15]. The mixed Al/Cu potential is expected to occur precisely within this passive range so that pit initiation is possible, although some repassivation phenomena are also expected. This would explain why a fairly generalized evolution of hydrogen was detected on bare aluminum (Fig. 13b), but activation-deactivation phenomena were observed after inhibitor treatment (see Fig. 13e and Fig. 13 f). It can be concluded that OPA, despite the decreased ability of the surface to donate electrons according to feedback mode experiments, is not a very effective inhibitor against localized corrosion attack on galvanically coupled Al/Cu.

4. Conclusions

Localized electrochemical activity on the Al/Cu substrate with and without treatment with 2-mercaptobenzimidazole (MBI) and octylphosphonic acid (OPA) was imaged using SECM and SVET under spontaneous corrosion potential conditions developed in the presence of an aggressive electrolyte containing chloride ions. Measurements of key redox species, namely oxygen and hydrogen, as well as ion fluxes, were performed as a function of elapsed time (*real-time*) and position on the surface under investigation (in situ).

The results revealed that it would be tempting to attribute the observation of localized increases in cathodic currents corresponding to a reduction of available dissolved oxygen at the tip (i.e., the concentration of oxygen remaining in the electrolyte which was not consumed at cathodic locations), to pit topography or some other localized surface depression. However, the methodology proposed in this work involving alternative monitoring of the concentration profiles of molecular hydrogen and dissolved oxygen ruled out the influence of topography and attributed it to the emergent redox sites. That is, at the sites on the aluminum surface where hydrogen evolves, ORR activity does not occur but is only noted in the immediate vicinity of the anodic sites. It was also observed that the Pt tip becomes ineffective over time when it was placed over a copper surface galvanically connected to aluminum during feedback mode measurements, a feature that we attribute to oxidation of the tip to $Pt(OH)_2$ due to the increase in pH of the adjacent electrolyte at sufficiently high potentials. To successfully avoid this unwanted effect in the tip, an experimental connection-disconnection procedure was developed.

Finally, the impressive corrosion resistance generated in the MBI solution – Al/Cu interface, which is established immediately upon immersion in a chloride solution containing MBI and increases to a higher level with immersion time, must be due to the formation of a protective Cu-MBI layer that effectively blocks the cathodic sites. More importantly, MBI exhibits excellent protection against localized corrosion, even in the chloride solution, which does not contain an MBI reservoir. On the other hand, OPA does not provide sufficient barrier properties against the penetration of aggressive ions such as chloride, based on the high faradaic currents detected at various locations on the Al surface, which are associated with the onset of pitting corrosion.

Funding

The Ph.D. scholarship for D.K.K. by Ad Futura through the Public scholarship, development, disability and maintenance fund of the Republic of Slovenia is acknowledged. D.K.K. also expresses his gratitude to the ERASMUS+ traineeship program for financially supporting a 3-month mobility grant to the University of La Laguna, Tenerife, Spain, during his doctoral studies. Funding by the Slovenian Research Agency (core program funding grants No. P2–0393 and P1–0134), and by the Spanish Ministry of Science and Innovation (MICINN, Madrid, Spain) and the European Regional Development Fund (Brussels, Belgium) MCIN/AEI/10.13039/501100011033/FEDER,UE under grant PID2021–127445NB-I00 is also acknowledged.

CRediT authorship contribution statement

Dževad K. Kozlica: Methodology, Experimental work, Data analysis, Writing – original draft. **Brenda Hernández-Concepción:** Experimental work. **Javier Izquierdo:** Conceptualization, Methodology, Writing – review & editing. **Ricardo M. Souto:** Conceptualization, Methodology, Writing – review & editing. **Ingrid Milošev**; Conceptualization, Methodology, Writing – review & editing.

Declaration of Competing Interest

The authors declare that they have no known competing financial interests or personal relationships that could have appeared to influence the work reported in this paper.

Data availability

Data will be made available on request.

Appendix A. Supporting information

Supplementary data associated with this article can be found in the online version at doi:10.1016/j.corsci.2023.111114.

References

[1] R.G. Buchheit, M.A. Martinez, L.P. Montes, Evidence for Cu ion formation by dissolution and dealloying the Al_2CuMg intermetallic compound in rotating ring-disk collection experiments, J. Electrochem. Soc. 141 (1) (2000) 119, https://doi.org/10.1149/1.1393164.

[2] M.A. Jakab, D.A. Little, J.R. Scully, Experimental and modeling studies of the oxygen reduction reaction on AA2024-T3, J. Electrochem. Soc. 152 (8) (2005) B311, https://doi.org/10.1149/1.1949047.

[3] R. Catubig, A.E. Hughes, I.S. Cole, F.F. Chen, C.M. MacRae, N.C. Wilson, A. M. Glenn, B.R.W. Hinton, M. Forsyth, The influence of rare earth mercaptoacetate on the initiation of corrosion on AA2024-T3 Part I: Average statistics of each intermetallic composition, Corros. Sci. 95 (2015), https://doi.org/10.1016/j.corsci.2015.01.056.

[4] Y. Ma, X. Zhou, W. Huang, G.E. Thompson, X. Zhang, C. Luo, Z. Sun, Localized corrosion in AA2099-T83 aluminum-lithium alloy: the role of intermetallic particles, Mater. Chem. Phys. 161 (2015) 201–210, https://doi.org/10.1016/j.matchemphys.2015.05.037.

[5] C. Luo, S.P. Albu, X. Zhou, Z. Sun, X. Zhang, Z. Tang, G.E. Thompson, Continuous and discontinuous localized corrosion of a 2xxx aluminium-copper-lithium alloy in sodium chloride solution, J. Alloy. Compd. 658 (2016) 61–70, https://doi.org/10.1016/j.jallcom.2015.10.185.

[6] J.V. de Sousa Araujo, U. Donatus, F.M. Queiroz, M. Terada, M.X. Milagre, M.C. de Alencar, I. Costa, On the severe localized corrosion susceptibility of the AA2198-T851 alloy, Corros. Sci. 133 (2018) 132–140, https://doi.org/10.1016/j.corsci.2018.01.028.

[7] I. Milošev, D. Zimerl, C. Carriére, S. Zanna, A. Seyeux, J. Iskra, S. Stavber, F. Chiter, M. Poberžnik, D. Costa, A. Kokalj, P. Marcus, The Effect of anchor group and alkyl backbone chain on performance of organic compounds as corrosion inhibitors for aluminum investigated using an integrative experimental-modeling approach, , J. Electrochem. Soc. 167 (2020), 061509, https://doi.org/10.1149/1945-7111/ab829d.

[8] R. Zhao, P. Rupper, S. Gaan, Recent development in phosphonic acid-based organic coatings on aluminum, Coatings 7 (2017) 133, https://doi.org/10.3390/coatings7090133.

[9] E. Hoque, J.A. Derose, G. Kulik, P. Hoffmann, H.J. Mathieu, B. Bhushan, Alkylphosphonate modified aluminum oxide surfaces, J. Phys. Chem. B 110 (2006) 10855–10861, https://doi.org/10.1021/jp061327a.

[10] V.S. Sastri, Green Corrosion Inhibitors: Theory and Practice, John Wiley & Sons, 2011, https://doi.org/10.1002/9781118015438.

[11] J. Li, C.W. Du, Z.Y. Liu, X.G. Li, M. Liu, Inhibition film formed by 2-mercapto-benzothiazole on copper surface and its degradation mechanism in sodium chloride solution, Int. J. Electrochem. Sci. 11 (2016) 10690–10705, https://doi.org/10.20964/2016.12.46.

[12] I. Milošev, N. Kovačević, J. Kovač, A. Kokalj, The roles of mercapto, benzene and methyl groups in the corrosion inhibition of imidazoles on copper: I. Experimental characterization, Corros. Sci. 98 (2015) 107–118, https://doi.org/10.1016/j.corsci.2015.05.006.

[13] A. Kokalj, S. Peljhan, M. Finšgar, I. Milošev, What determines the inhibition effectiveness of ATA, BTAH, and BTAOH corrosion inhibitors on copper? J. Am. Chem. Soc. 132 (2010) 16657–16668, https://doi.org/10.1021/ja107704y.

[14] D.K. Kozlica, I. Milošev, Corrosion inhibition of copper and aluminium by 2-mercaptobenzimidazole and octylphosphonic acid – surface pre-treatment and method of film preparation, Electrochim. Acta 431 (2022), 141154, https://doi.org/10.1016/j.electacta.2022.141154.

[15] D.K. Kozlica, A. Kokalj, I. Milošev, Synergistic effect of 2-mercaptobenzimidazole and octylphosphonic acid as corrosion inhibitors for copper and aluminium – an electrochemical, XPS, FTIR and DFT study, Corros. Sci. 182 (2021), 109082, https://doi.org/10.1016/j.corsci.2020.109082.

[16] D.K. Kozlica, J. Ekar, J. Kovač, I. Milošev, Roles of chloride ions in the formation of corrosion protective films on copper, J. Electrochem. Soc. 168 (2021), 031504, https://doi.org/10.1149/1945-7111/abe34a.

[17] A.J. Bard, F.R.F. Fan, J. Kwak, O. Lev, Scanning electrochemical microscopy. Introduction and principles, Anal. Chem. 61 (1989) 132–138, https://doi.org/10.1021/ac00177a011.

[18] A.J. Bard, F.R.F. Fan, D.T. Pierce, P.R. Unwin, D.O. Wipf, F. Zhou, Chemical imaging of surfaces with the scanning electrochemical microscope, Science 254 (1991) 68–74, https://doi.org/10.1126/science.254.5028.68.

[19] A.J. Bard, M.V. Mirkin. Scanning electrochemical microscopy, second ed., CRS Press, New York, 2001.

[20] D. Snihirova, M. Taryba, S.V. Lamaka, M.F. Montemor, Corrosion inhibition synergies on a model Al-Cu-Mg sample studied by localized scanning electrochemical techniques, Corros. Sci. 112 (2016) 408–417, https://doi.org/10.1016/j.corsci.2016.08.008.

[21] H. Shi, E.H. Han, F. Liu, T. Wei, Z. Zhu, D. Xu, Study of corrosion inhibition of coupled Al_2Cu-Al and Al_3Fe-Al by cerium cinnamate using scanning vibrating electrode technique and scanning ion-selective electrode technique, Corros. Sci. 98 (2015) 150–162, https://doi.org/10.1016/j.corsci.2015.05.019.

[22] A.M. Simões, A.C. Bastos, M.G. Ferreira, Y. González-García, S. González, R. M. Souto, Use of SVET and SECM to study the galvanic corrosion of an iron-zinc cell, Corros. Sci. 49 (2007) 726–739, https://doi.org/10.1016/j.corsci.2006.04.021.

[23] R.M. Souto, Y. González-García, A.C. Bastos, A.M. Simões, Investigating corrosion processes in the micrometric range: a SVET study of the galvanic corrosion of zinc coupled with iron, Corros. Sci. 49 (2007) 4568–4580, https://doi.org/10.1016/j.corsci.2007.04.016.

[24] L.B. Coelho, M. Mouanga, M.E. Druart, I. Recloux, D. Cossement, M.G. Olivier, A SVET study of the inhibitive effects of benzotriazole and cerium chloride solely and combined on an aluminium/copper galvanic coupling model, Corros. Sci. 110 (2016) 143–156, https://doi.org/10.1016/j.corsci.2016.04.036.

[25] J.A. Ramírez-Cano, L. Veleva, R.M. Souto, B.M. Fernández-Pérez, Investigating metal-inhibitor interaction with EQCM and SVET: 3-amino-1,2,4-triazole on Au, Cu and Au–Cu galvanic coupling, Mater. Corros. 69 (2018) 115–124, https://doi.org/10.1002/maco.201709564.

[26] J.A. Ramírez-Cano, L. Veleva, B.M. Fernández-Pérez, R.M. Souto, SVET study of the interaction of 2-Mercaptobenzothiazole corrosion inhibitor with Au, Cu And Au-Cu galvanic pair, Int. J. Corros. Scale Inhib. 6 (2017) 307–317, https://doi.org/10.17675/2305-6894-2017-6-3-6.

[27] J. Izquierdo, L. Nagy, J.J. Santana, G. Nagy, R.M. Souto, A novel microelectrochemical strategy for the study of corrosion inhibitors employing the scanning vibrating electrode technique and dual potentiometric/amperometric operation in scanning electrochemical microscopy: application to the study of the cathodic inhibition by benzotriazole of the galvanic corrosion of copper coupled to iron, Electrochim. Acta 58 (2011) 707–716, https://doi.org/10.1016/j.electacta.2011.10.027.

[28] J.-B. Jorcin, C. Blanc, N. Pebere, B. Tribollet, V. Vivier, Galvanic coupling between pure copper and pure aluminum: experimental approach and mathematical model, J. Electrochem. Soc. 155 (2008) C46.

[29] X. Joseph Raj, T. Nishimura, Studies on galvanic corrosion of iron–magnesium couple by scanning electrochemical microscopy in 0.1 M NaCl solution, J. Ind. Eng. Chem. 41 (2016) 141–150, https://doi.org/10.1016/j.jiec.2016.07.020.

[30] J.R. Xavier, Galvanic corrosion of copper/titanium in aircraft structures using a cyclic wet/dry corrosion test in marine environment by EIS and SECM techniques, SN Appl. Sci. 2 (2020) 1341, https://doi.org/10.1007/s42452-020-3145-x.

[31] D. Filotás, B.M. Fernández-Pérez, J. Izquierdo, A. Kiss, L. Nagy, G. Nagy, R. M. Souto, Improved potentiometric SECM imaging of galvanic corrosion reactions, Corros. Sci. 129 (2017) 136–145, https://doi.org/10.1016/j.corsci.2017.10.006.

[32] J. Izquierdo, L. Nagy, S. González, J.J. Santana, G. Nagy, R.M. Souto, Resolution of the apparent experimental discrepancies observed between SVET and SECM for the characterization of galvanic corrosion reactions, Electrochem. Commun. 27 (2013) 50–53, https://doi.org/10.1016/j.elecom.2012.11.002.

[33] A.C. Bastos, M.C. Quevedo, O.V. Karavai, M.G.S. Ferreira, Review – On the application of the scanning vibrating electrode technique (SVET) to corrosion research, J. Electrochem. Soc. 164 (2017) C973–C990, https://doi.org/10.1149/2.0431714jes.

[34] D. Snihirova, D. Höche, S. Lamaka, Z. Mir, T. Hack, M.L. Zheludkevich, Galvanic corrosion of Ti6Al4V -AA2024 joints in aircraft environment: modelling and experimental validation, Corros. Sci. 157 (2019) 70–78, https://doi.org/10.1016/j.corsci.2019.04.036.

[35] J. Izquierdo, J.J. Santana, S. González, R.M. Souto, Scanning microelectrochemical characterization of the anti-corrosion performance of inhibitor films formed by 2-mercaptobenzimidazole on copper, Prog. Org. Coat. 74 (2012) 526–533, https://doi.org/10.1016/j.porgcoat.2012.01.019.

[36] S.Y. Yu, W.E. O'Grady, D.E. Ramaker, P.M. Natishan, Chloride ingress into aluminum prior to pitting corrosion An investigation by XANES and XPS, J. Electrochem. Soc. 147 (2000), https://doi.org/10.1149/1.1393630.

[37] P. Marcus, V. Maurice, H.H. Strehblow, Localized corrosion (pitting): A model of passivity breakdown including the role of the oxide layer nanostructure, Corros. Sci. 50 (2008) 2698–2704, https://doi.org/10.1016/j.corsci.2008.06.047.

[38] G.T. Burstein, C. Liu, R.M. Souto, S.P. Vines, Origins of pitting corrosion, Corros. Eng. Sci. Technol. 39 (2004) 25–30, https://doi.org/10.1179/147842204225016859.

[39] T.R. Beck, Salt film formation during corrosion of aluminum, Electrochim. Acta 29 (1984) 485–491, https://doi.org/10.1016/0013-4686(84)87098-X.

[40] Y. González-García, G.T. Burstein, S. González, R.M. Souto, Imaging metastable pits on austenitic stainless steel in situ at the open-circuit corrosion potential, Electrochem. Commun. 6 (2004) 637–642, https://doi.org/10.1016/j.elecom.2004.04.018.

[41] A. Boag, R.J. Taylor, T.H. Muster, N. Goodman, D. McCulloch, C. Ryan, B. Rout, D. Jamieson, A.E. Hughes, Stable pit formation on AA2024-T3 in a NaCl environment, Corros. Sci. 52 (2010) 90–103, https://doi.org/10.1016/j.corsci.2009.08.043.

[42] M. Curioni, F. Scenini, The mechanism of hydrogen evolution during anodic polarization of aluminium, Electrochim. Acta 180 (2015) 712–721, https://doi.org/10.1016/j.electacta.2015.08.076.

[43] G.S. Frankel, The growth of 2-D pits in thin film aluminum, Corros. Sci. 30 (1990) 1203–1218, https://doi.org/10.1016/0010-938X(90)90199-F.

[44] Z. Szklarska-Smialowska, Pitting corrosion of aluminum, Corros. Sci. 41 (1999) 1743–1767.

[45] D. Chadwick, T. Hashemi, Electron spectroscopy of corrosion inhibitors: surface films formed by 2-mercaptobenzothiazole and 2-mercaptobenzimidazole on copper, Surf. Sci. 89 (1979) 649–659, https://doi.org/10.1016/0039-6028(79)90646-0.
[46] G. Xue, X.Y. Huang, J. Dong, J. Zhang, The formation of an effective anti-corrosion film on copper surfaces from 2-mercaptobenzimidazole solution, J. Electroanal. Chem. 310 (1991) 139–148, https://doi.org/10.1016/0022-0728(91)85257-P.
[47] M. Finšgar, 2-Mercaptobenzimidazole as a copper corrosion inhibitor: part II. Surface analysis using X-ray photoelectron spectroscopy, Corros. Sci. 72 (2013) 90–98, https://doi.org/10.1016/j.corsci.2013.03.010.
[48] T. Hauffman, O. Blajiev, J. Snauwaert, C. Van Haesendonck, A. Hubin, H. Terryn, Study of the self-assembling of n-octylphosphonic acid layers on aluminum oxide, Langmuir 24 (2008) 13450–13456, https://doi.org/10.1021/la801978a.
[49] C. Lefrou, R. Cornut, Analytical expressions for quantitative scanning electrochemical microscopy (SECM), ChemPhysChem 11 (2010) 547–556, https://doi.org/10.1002/cphc.200900600.
[50] R. Cornut, C. Lefrou, New analytical approximation of feedback approach curves with a microdisk SECM tip and irreversible kinetic reaction at the substrate, J. Electroanal. Chem. 621 (2008) 178–184, https://doi.org/10.1016/j.jelechem.2007.09.021.
[51] U.M. Tefashe, M.E. Snowden, P.D. Ducharme, M. Danaie, G.A. Botton, J. Mauzeroll, Local flux of hydrogen from magnesium alloy corrosion investigated by scanning electrochemical microscopy, J. Electroanal. Chem. 720–721 (2014) 121–127, https://doi.org/10.1016/j.jelechem.2014.03.002.
[52] R.M.P. da Silva, J. Izquierdo, M.X. Milagre, A.M. Betancor-Abreu, I. Costa, R. M. Souto, Use of amperometric and potentiometric probes in scanning electrochemical microscopy for the spatially-resolved monitoring of severe localized corrosion sites on aluminum alloy 2098-t351, Sensors 21 (2021) 1–15, https://doi.org/10.3390/s21041132.
[53] C.B. Bargeron, R.C. Benson, Analysis of the gases evolved during the pitting corrosion of aluminum in various electrolytes, J. Electrochem. Soc. 127 (1980) 2528–2530, https://doi.org/10.1149/1.2129511.
[54] D.M. Dražić, J. Popić, Hydrogen evolution on aluminium in chloride solutions, J. Electroanal. Chem. 357 (1993) 105–116, https://doi.org/10.1016/0022-0728(93)80377-T.
[55] C. Laurent, F. Scenini, T. Monetta, F. Bellucci, M. Curioni, The contribution of hydrogen evolution processes during corrosion of aluminium and aluminium alloys investigated by potentiodynamic polarisation coupled with real-time hydrogen measurement, Npj Mater. Degrad. 1 (2017) 6, https://doi.org/10.1038/s41529-017-0011-4.
[56] G.S. Frankel, S. Fajardo, B.M. Lynch, Introductory lecture on corrosion chemistry: a focus on anodic hydrogen evolution on Al and Mg, Faraday Discuss. 180 (2015) 11–33, https://doi.org/10.1039/c5fd00066a.
[57] J. Izquierdo, A. Eifert, C. Kranz, R.M. Souto, In situ investigation of copper corrosion in acidic chloride solution using atomic force-scanning electrochemical microscopy, Electrochim. Acta 247 (2017) 588–599, https://doi.org/10.1016/j.electacta.2017.07.042.
[58] J. Izquierdo, A. Eifert, R.M. Souto, C. Kranz, Simultaneous pit generation and visualization of pit topography using combined atomic force-scanning electrochemical microscopy, Electrochem. Commun. 51 (2015) 15–18, https://doi.org/10.1016/j.elecom.2014.11.017.
[59] M.J.N. Pourbaix, Atlas of Electrochemical Equilibria in Aqueous Solutions, Pergamon, Oxford, 1966.
[60] I. Milošev, T. Bakarič, S. Zanna, A. Seyeux, P. Rodič, M. Poberžnik, F. Chiter, P. Cornette, D. Costa, A. Kokalj, P. Marcus, Electrochemical, surface-analytical, and computational DFT study of alkaline etched aluminum modified by carboxylic acids for corrosion protection and hydrophobicity, J. Electrochem. Soc. 166 (2019) C3131, https://doi.org/10.1149/2.0181911jes.